Graph Reduction of Complex Energy-Integrated Networks: Process Systems Applications

Seongmin Heo, Srinivas Rangarajan, and Prodromos Daoutidis
Dept. of Chemical Engineering and Materials Science, University of Minnesota, Minneapolis, MN 55455

Sujit S. Jogwar
Dept. of Chemical Engineering, Institute of Chemical Technology, Matunga, Mumbai 400019 India

DOI 10.1002/aic.14341
Published online January 23, 2014 in Wiley Online Library (wileyonlinelibrary.com)

We illustrate the application of a graph reduction method developed recently to analyze complex energy-integrated process networks. The method uses information on the energy flow structure of the network and the orders of magnitude of the different energy flows to generate, automatically, information on the time scales where the process units evolve, canonical forms of the reduced models in each time scale, and controlled variables and potential manipulated inputs available in each time scale. Representative examples of reactor-heat exchanger and distillation column networks are considered to illustrate the method and develop insights on effective control strategies for these processes. © 2014 American Institute of Chemical Engineers *AIChE J*, 60: 995–1012, 2014
Keywords: process control, simulation, process

Introduction

High energy efficiency has become a critical need in modern chemical plants. Energy integration has been an active topic of research,[1,2] as it enables reduction in external utility consumption and, thus, provides cost benefits. It involves coupling of heating and cooling requirements of a plant to transfer energy from an energy source to an energy sink. However, energy-integrated chemical plants are difficult to operate and control, especially in the context of transitions between different operating points. Several analysis and control approaches have been recently proposed for such process networks. These include passivity/dissipativity-based methods,[3–5] distributed control,[6,7] quasi-decentralized control,[8,9] plantwide control,[10,11] and hierarchical control.[12,13]

In previous work,[12,14] we have identified two prototype energy-integrated networks, those with large energy recycle compared to the external energy flows, and those with large energy throughput. The disparate magnitudes of energy flows in such networks were shown to be at the origin of a two-time scale behavior and a segregation of flows that can be used as manipulated inputs in the different time scales. Exploiting these features, we developed model reduction methods using singular perturbations and a hierarchical control strategy wherein different control objectives are addressed in different time scales.

In practice, complex energy-integrated chemical plants consist of combinations of energy recycle and energy throughput networks, often with large energy flows, thus showing the potential of multi-time scale energy dynamics.[15] A detailed mathematical analysis through successive application of singular perturbations can, in principle, be used to analyze such networks. However, such an analysis becomes cumbersome as the size of the network increases. To this end, we have proposed a generic and scalable graph-theoretic framework which can be used to analyze such networks.[16,17] The developed framework relies on knowledge of the energy flow structure in the network and the orders of magnitude of the different energy flows to generate information on (1) the time scales where each unit evolves, (2) the form of the reduced order models in each time scale, and (3) controlled outputs and potential manipulated inputs available in each time scale. Such information allows us to develop a hierarchical control strategy for such networks.

In the present work, we consider two different classes of such networks which are common in process systems: reactor-heat exchanger networks and energy-integrated distillation column networks. For representative cases of such networks, we illustrate the application of the graph reduction method, compare it with the analytical, singular perturbations-based reduction, and identify and discuss insights on the dynamic structure of such networks that affect their control.

Graph Reduction for Complex Energy-Integrated Networks

In this section, we describe briefly the main features of the developed graph reduction framework (for details see the Refs. 16, 17).

The energy dynamics of a generic complex energy-integrated network, which consists of N units and energy flows, h_i, spanning m orders of magnitude, can be described by the following equations

Correspondence concerning this article should be addressed to P. Daoutidis at daout001@umn.edu.

$$\frac{d\mathbf{H}}{dt}=\sum_{i=0}^{m-1}\frac{1}{\varepsilon_i}\mathbf{F}_i\mathbf{g}_i(\mathbf{H},\mathbf{u}_i) \quad (1)$$

where the energy flows of different orders of magnitude are indexed by i. ε_i are small parameters, which are defined as ratios of nominal steady state flows ($\varepsilon_i=h_{0,s}/h_{i,s}$), such that $\varepsilon_i \ll 1$ and $\varepsilon_{i+1}/\varepsilon_i \ll 1$. In the subsequent analyses, we assume ε_0 to be equal to 1. $\mathbf{H}$ is the vector of enthalpy of the N process units, $\mathbf{g}_i$ are vectors with contributions from the energy flows of $\mathcal{O}(1/\varepsilon_i)$, and $\mathbf{F}_i$ are the corresponding selector matrices such that $\mathbf{F}_i(j,k)=1$ if the energy balance equation of the unit k includes the j-th element of $\mathbf{g}_i$ and 0 otherwise. $\mathbf{u}_i$ represent scaled energy flows that can be used as manipulated variables.

Note that Eq. 1 is a singularly perturbed system with multiple small parameters. Model reduction can be performed sequentially by considering each time scale $\tau_i=t/\varepsilon_i$ (starting from the fastest) and setting the small parameter ε_i to 0, to obtain reduced models of the slow and fast dynamics in this time scale. For each time scale τ_i, the description of the dynamics can be obtained in the limit $\varepsilon_i \to 0$ as

$$\frac{d\mathbf{H}_i}{d\tau_i}=(\mathbf{F}_i^T\mathbf{F}_i)\hat{\mathbf{g}}_i(\mathbf{H}_i\mathbf{u}_i)$$

where $\mathbf{H}_i=\mathbf{F}_i^T\mathbf{H}$ represent the unit enthalpies evolving in the time scale τ_i, and $\hat{\mathbf{g}}_i$ represents the correspondingly adjusted vector. Quasi-steady state constraints for the time scale τ_i can be identified as $\hat{\mathbf{g}}_i(\mathbf{H}_i,\mathbf{u}_i)=0$. Differentiating these constraints with respect to time, we obtain

$$0=\frac{\partial\hat{\mathbf{g}}_i}{\partial t}=\frac{\partial\hat{\mathbf{g}}_i}{\partial\mathbf{H}_i}\frac{d\mathbf{H}_i}{dt}$$

If the constraints are linearly independent, the matrix $\partial\hat{\mathbf{g}}_i/\partial\mathbf{H}_i$ is nonsingular, and we get $d\mathbf{H}_i/dt=0$. This implies that the enthalpies $\mathbf{H}_i$ evolve only in the time scale τ_i and not in slower ones. If the constraints are linearly dependent, the matrix $\partial\hat{\mathbf{g}}_i/\partial\mathbf{H}_i$ becomes singular, and the i-th time scale dynamics of $\mathbf{H}_i$ are accompanied by a slower evolution in subsequent time scales. The model of the slower dynamics in this case is an index two differential algebraic equation (DAE) system with the dynamic equations being the differential equations, the quasi-steady state constraints being the algebraic equations, and the limiting terms $\lim_{\varepsilon_i\to 0}\tilde{\mathbf{g}}_i/\varepsilon_i$ being the algebraic variables, where $\tilde{\mathbf{g}}_i$ represents the linearly independent subset of the quasi-steady state constraints. Large throughputs, splitting, and mixing structures give rise to linearly independent constraints,[14] whereas large recycles give rise to linearly dependent constraints.[12]

The above reduction can be performed in a graph-theoretic framework. The energy flow structures of complex energy-integrated process networks can be represented as *energy flow graphs* with nodes corresponding to the individual units of the networks, and directed and weighted edges corresponding to the energy flows. In this setting, energy recycles and throughputs are energy flow cycles and energy flow paths, respectively. Energy flows with different orders of magnitude can be distinguished by using lines of different thickness (corresponding to different edge weights) in such graphs. Also, we use nodes with solid borders to represent normal nodes (i.e., nodes for the process units), and nodes with dashed borders to represent auxiliary nodes (i.e., nodes for external energy sources/sinks).

Figure 1a shows an energy flow graph for a large recycle network. Such networks can be equivalently represented as a single composite node R. Figure 1b shows an energy flow graph of a network with large energy throughput. The units in such networks can be clustered to form a single composite node T. Such clustering reduces the complexity in the representation of the networks and facilitates graph reduction. In the following sections, networks with large energy recycle and networks with large energy throughput will be referred to as *prototype recycle* and *prototype throughput*, respectively.

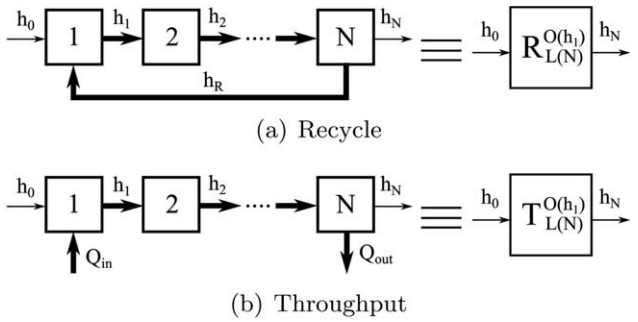

Figure 1. Composite units for prototype networks.

The algorithm for the graph-theoretic analysis is included in Appendix (adopted from the Ref. 17). The algorithm has been implemented as a computational tool written in C++ to automate this graph reduction analysis and has been used in all examples studied herein. In what follows, we briefly describe the graph reduction and analysis method and its implementation through the algorithm.

Complex networks comprise of combinations of energy recycles and throughputs, some of which are prototype. The developed graph reduction method begins with a user specified classification of the energy flows in classes of distinct orders of magnitude, W. Starting with the largest flows which correspond to the fastest dynamics, and proceeding to all subsequent classes of flows, it first extracts a *subgraph*, using the subroutine *InducedSubgraph*, corresponding to each time scale. It thus identifies the units evolving in each time scale (those with nodes in that subgraph) and proceeds to identify prototype patterns, using the subroutine *SmallestElementaryCycle*, and simplify them through clustering using the subroutine *GraphReduce*. Throughput blocks are removed from the original energy flow graph, before proceeding to the subsequent time scales, as the energy dynamics of all the units of prototype throughputs evolve in a single time scale.

Next, it constructs the canonical forms of the original full order dynamic model as well as the reduced order dynamic models for the energy balance variables (enthalpies) in each time scale. The energy balance equations for the full order model (or the reduced models) are derived based on the connectivity information of the energy flow graph (or subgraph) using the subroutine *Ebalance*. For the reduced model, the method also predicts the linear independency of the quasi-steady state constraints from the existence of auxiliary nodes connected to individual composite nodes. Specifically, if there exists no auxiliary node connected to a composite node in a subgraph, the quasi-steady state constraints resulting from the corresponding dynamic model of that composite node are linearly dependent. In this case, the composite node is added to the set *PureRecycles* and the corresponding time scale is added to the set *RecycleTimes*. For a specific time scale, *Constraint* represents the linearly independent constraints obtained from the previous time scale, and DAE represents the contribution of the previous time scale dynamics to the current time scale dynamics.

Finally, the method classifies the control objectives and the manipulated inputs available in each time scale. Specifically, the enthalpy of any node in a subgraph can be controlled in the corresponding time scale using any edge in the same subgraph as the manipulated input. Note that if a composite node does not have any auxiliary node connected to it (i.e., a prototype recycle composite node), one cannot simultaneously control the enthalpies of all the units, comprising that composite node, as the dynamic equations in this case are linearly dependent. Thus, all but one of the units for such a composite node can be controlled in the corresponding time scale, and the remaining unit can be controlled in the subsequent time scale.

To present the results obtained from the graph-theoretic analysis, we use the following notations:

1. τ_i: The i-th time scale defined by t/ε_i, where ε_i is a small parameter.
2. $\mathcal{G}$: The original energy flow graph of the network.
3. $\mathcal{H}_i$: The subgraph of $\mathcal{G}$ corresponding to the time scale τ_i. It contains all and only the energy flows of the order of magnitude i.
4. $\mathcal{T}(\tau_i)$: The set of nodes whose enthalpy evoles in the time scale τ_i.
5. $\mathcal{Y}(\tau_i)$: The set of nodes whose enthalpy can be controlled in the time scale τ_i.
6. $\mathcal{U}(\tau_i)$: The set of edges which can be used as a manipulated input in the time scale τ_i.

In what follows, we analyze relevant example chemical process networks using this graph-theoretic framework.

Energy-Integrated Reactor-Heat Exchanger Networks

For processes with high temperature reactions, there are opportunities for energy integration as the outlet stream of the reactor, which is at high temperature, can be used to provide energy to other process streams; such integration can be achieved through heat exchangers, thus forming reactor-heat exchanger networks. In what follows, we analyze two typical examples of such networks.

Toluene hydrodealkylation process

Process Description. Let us consider a design alternative (alternative 1) of the toluene hydrodealkylation (HDA) process proposed by Terrill and Douglas[18] as shown in Figure 2. In this process, the reactant mixture is preheated in a feed-effluent heat exchanger (FEHE), where the mixture is completely vaporized, and is further heated using a furnace. It is then fed to an adiabatic plug-flow reactor where the following reactions occur

$$C_6H_5CH_3 + H_2 \rightarrow C_6H_6 + CH_4 \quad \text{Reaction 1}$$
$$2C_6H_6 \rightleftharpoons (C_6H_5)_2 \quad \text{Reaction 2}$$

where benzene, which is the main product of the process, is produced through an irreversible exothermic reaction ($\Delta H_1 = -41.826$ kJ/mol). The reactor effluent is cooled using the FEHE and the cooler, and is fed to the separator. A majority of the vapor outlet of the separator is compressed, and fed back to the reactor, while the residual vapor stream is purged. The liquid outlet of the separator goes through a series of distillation columns. In the stabilizer column, hydrogen and methane gas are removed from the liquid stream. In the product column, benzene product is produced as the distillate. Diphenyl is the bottoms of the recycle column, and the distillate of the recycle column, which is the unreacted toluene, is recycled.

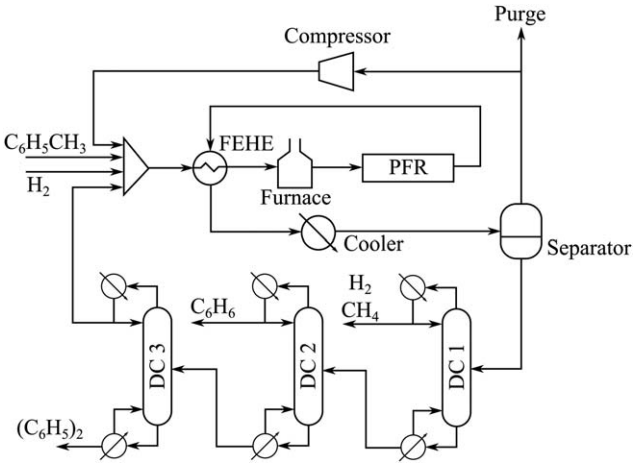

Figure 2. Toluene hydrodealkylation process.

We first perform the detailed mathematical analysis using singular perturbations as the model reduction tool. Then, the graph-theoretic analysis is applied, and the results are compared. Finally, via numerical simulations, the energy dynamics of the process is investigated to confirm the analysis results.

Detailed Analysis. In this analysis, we focus on the reaction part of the process, where we observe the following features, which give rise to a potential of multi-time scale energy dynamics:

1. The reactant mixture is completely vaporized in the FEHE, indicating that a large amount of energy is recovered through the FEHE.
2. There is a large material recycle fed back to the reactor.

Remark 1. *Note that the separation part of the network, which consists of three distillation columns, is not included in the analysis. The reason is that the energy integration in that part is dominated by large energy throughputs, which do not lead to time scale multiplicity in the energy dynamics. More detailed justification and examples of energy-integrated distillation column networks that lead to time scale multiplicity in the energy dynamics can be found in the subsequent section.*

The governing equations of the energy dynamics of the network can be written as follows

$$\begin{aligned}
\frac{dT_m}{dt} &= \frac{R(T_{cp}-T_m)}{V_m} + \frac{F_{tf}(T_{tf}-T_m)}{V_m} + \frac{F_{hf}(T_{hf}-T_m)}{V_m} + \frac{F_{tr}(T_{tr}-T_m)}{V_m} \\
\frac{dT_c}{dt} &= \frac{F(T_m-T_c)}{V_c} + \frac{Q_{\text{rec}}}{\rho C_p V_c} \\
\frac{dT_f}{dt} &= \frac{F(T_c-T_f)}{V_f} + \frac{Q_f}{\rho C_p V_f} \\
\frac{dT_r}{dt} &= \frac{F(T_f-T_r)}{V_r} - \frac{\Delta \mathbf{H}\cdot \mathbf{r}}{\rho C_p} \\
\frac{dT_h}{dt} &= \frac{F(T_r-T_h)}{V_h} - \frac{Q_{\text{rec}}}{\rho C_p V_h} \\
\frac{dT_{cl}}{dt} &= \frac{F(T_h-T_{cl})}{V_{cl}} - \frac{Q_{cl}}{\rho C_p V_{cl}} \\
\frac{dT_{sp}}{dt} &= \frac{R(T_{cl}-T_{sp})}{V_{sp}} + \frac{F_P(T_{cl}-T_{sp})}{V_{sp}} + \frac{F_l(T_{cl}-T_{sp})}{V_{sp}} \\
\frac{dT_{cp}}{dt} &= \frac{R(T_{sp}-T_{cp})}{V_{cp}} + \frac{W}{\rho C_p V_{cp}}
\end{aligned} \tag{2}$$

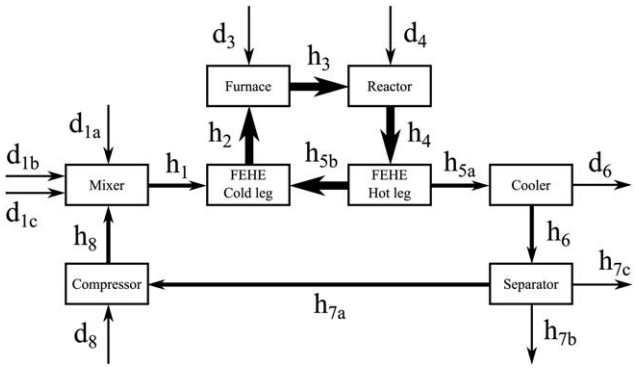

Figure 3. Energy representation of the reaction part of the HDA process.

with

$$F = R + F_{tf} + F_{hf} + F_{tr}$$

$$Q_{\text{rec}} = UA\frac{(T_r - T_c) - (T_h - T_m)}{ln[(T_r - T_c)/(T_h - T_m)]}$$

where the subscripts m, c, f, r, h, cl, sp and cp are used to represent the mixer, the cold channel of the FEHE, the furnace, the reactor, the hot channel of the FEHE, the cooler, the separator, and the compressor, respectively. Also, subscripts tf, hf and tr are used for the toluene feed stream, the hydrogen feed stream and the toluene recycle stream, respectively. V is the volume of the unit, and Q is the duty. F is the volumetric flow rate, and R is the volumetric flow rate of the gas recycle. W is the power input to the compressor. U represents the overall heat-transfer coefficient and A is the heat-transfer area. $\Delta\mathbf{H} = [\Delta H_1, \Delta H_2]^T$ is the vector of the heats of reaction and $\mathbf{r} = [r_1, r_2]^T$ is the vector of the reaction rates, where the subscripts 1 and 2 correspond to the reaction 1 and reaction 2, respectively.

The energy representation of the reaction part of the network is shown in Figure 3. The orders of magnitude of the energy flows are determined based on the sensible heat content of the flows as shown in Table 1. ε_1 and ε_2 are small parameters ($\varepsilon_2 \ll \varepsilon_1 \ll 1$), which are the ratios of the energy input through the toluene feed stream (d_{1a}) to the rate of energy recycle through the gas recycle (h_8) and the rate of energy transferred inside the FEHE (h_{5b}), respectively, that is

$$\varepsilon_1 = \frac{[F_{tf}\rho C_p(T_{tf} - T_{\text{ref}})]_s}{[R\rho C_p(T_{cp} - T_{\text{ref}})]_s}$$

$$\varepsilon_2 = \frac{[F_{tf}\rho C_p(T_{tf} - T_{\text{ref}})]_s}{Q_{rec,s}}$$

where T_{ref} is a reference temperature, and subscript s represents a steady state value.

We define the $\mathcal{O}(1)$ steady state ratios

$$k_{hf} = \frac{[F_{hf}\rho C_p(T_{hf} - T_{\text{ref}})]_s}{[F_{tf}\rho C_p(T_{tf} - T_{\text{ref}})]_s} \qquad k_{tr} = \frac{[F_{tr}\rho C_p(T_{tr} - T_{\text{ref}})]_s}{[F_{tf}\rho C_p(T_{tf} - T_{\text{ref}})]_s}$$

$$k_{qf} = \frac{Q_{f,s}}{[F_{tf}\rho C_p(T_{tf} - T_{\text{ref}})]_s} \qquad k_{hr} = \frac{[\Delta\mathbf{H}\cdot\mathbf{r}V_r]_s}{[F_{tf}\rho C_p(T_{tf} - T_{\text{ref}})]_s}$$

$$k_{qcl} = \frac{Q_{cl,s}}{[F_{tf}\rho C_p(T_{tf} - T_{\text{ref}})]_s} \qquad k_P = \frac{[F_P\rho C_p(T_s - T_{\text{ref}})]_s}{[F_{tf}\rho C_p(T_{tf} - T_{\text{ref}})]_s}$$

$$k_l = \frac{[F_l\rho C_p(T_s - T_{\text{ref}})]_s}{[F_{tf}\rho C_p(T_{tf} - T_{\text{ref}})]_s} \qquad k_w = \frac{W_s}{[F_{tf}\rho C_p(T_{tf} - T_{\text{ref}})]_s}$$

$$k_m = \frac{[F\rho C_p(T_m - T_{\text{ref}})]_s}{[R\rho C_p(T_{cp} - T_{\text{ref}})]_s} \qquad k_h = \frac{[F\rho C_p(T_h - T_{\text{ref}})]_s}{[R\rho C_p(T_{cp} - T_{\text{ref}})]_s}$$

$$k_{cl} = \frac{[F\rho C_p(T_{cl} - T_{\text{ref}})]_s}{[R\rho C_p(T_{cp} - T_{\text{ref}})]_s} \qquad k_{sp} = \frac{[R\rho C_p(T_{sp} - T_{\text{ref}})]_s}{[R\rho C_p(T_{cp} - T_{\text{ref}})]_s}$$

$$k_c = \frac{[F\rho C_p(T_c - T_{\text{ref}})]_s}{Q_{\text{rec},s}} \qquad k_f = \frac{[F\rho C_p(T_f - T_{\text{ref}})]_s}{Q_{\text{rec},s}}$$

$$k_r = \frac{[F\rho C_p(T_r - T_{\text{ref}})]_s}{Q_{\text{rec},s}}$$

and $\mathcal{O}(1)$ scaled energy flows

$$u_{tf} = \frac{F_{tf}\rho C_p(T_{tf} - T_{\text{ref}})}{[F_{tf}\rho C_p(T_{tf} - T_{\text{ref}})]_s} \qquad u_{hf} = \frac{F_{hf}\rho C_p(T_{hf} - T_{\text{ref}})}{[F_{hf}\rho C_p(T_{hf} - T_{\text{ref}})]_s}$$

$$u_{tr} = \frac{F_{tr}\rho C_p(T_{tr} - T_{\text{ref}})}{[F_{tr}\rho C_p(T_{tr} - T_{\text{ref}})]_s} \qquad u_{qf} = \frac{Q_f}{Q_{f,s}}$$

$$u_{hr} = \frac{\Delta\mathbf{H}\cdot\mathbf{r}V_r}{[\Delta\mathbf{H}\cdot\mathbf{r}V_r]_s} \qquad u_{qcl} = \frac{Q_{cl}}{Q_{cl,s}}$$

$$u_P = \frac{F_P\rho C_p(T_s - T_{\text{ref}})}{[F_P\rho C_p(T_s - T_{\text{ref}})]_s} \qquad u_l = \frac{F_l\rho C_p(T_s - T_{\text{ref}})}{[F_l\rho C_p(T_s - T_{\text{ref}})]_s}$$

$$u_w = \frac{W}{W_s} \qquad u_{cp} = \frac{R\rho C_p(T_{cp} - T_{\text{ref}})}{[R\rho C_p(T_{cp} - T_{\text{ref}})]_s}$$

$$u_m = \frac{F\rho C_p(T_m - T_{\text{ref}})}{[F\rho C_p(T_m - T_{\text{ref}})]_s} \qquad u_h = \frac{F\rho C_p(T_h - T_{\text{ref}})}{[F\rho C_p(T_h - T_{\text{ref}})]_s}$$

$$u_{cl} = \frac{F\rho C_p(T_{cl} - T_{\text{ref}})}{[F\rho C_p(T_{cl} - T_{\text{ref}})]_s} \qquad u_{sp} = \frac{R\rho C_p(T_{sp} - T_{\text{ref}})}{[R\rho C_p(T_{sp} - T_{\text{ref}})]_s}$$

$$u_{q\text{rec}} = \frac{Q_{\text{rec}}}{Q_{\text{rec},s}} \qquad u_c = \frac{F\rho C_p(T_c - T_{\text{ref}})}{[F\rho C_p(T_c - T_{\text{ref}})]_s}$$

$$u_f = \frac{F\rho C_p(T_f - T_{\text{ref}})}{[F\rho C_p(T_f - T_{\text{ref}})]_s} \qquad u_r = \frac{F\rho C_p(T_r - T_{\text{ref}})}{[F\rho C_p(T_r - T_{\text{ref}})]_s}$$

The energy dynamics equations in 2 thus become

Table 1. Summary of Orders of Magnitude of the Energy Flows of the HDA Process Reaction Part

Energy Flow	mC_pT(kW)	Order of Magnitude
h_1	6676	$\mathcal{O}(1/\varepsilon_1)$
h_2	33183	$\mathcal{O}(1/\varepsilon_2)$
h_3	33746	$\mathcal{O}(1/\varepsilon_2)$
h_4	36036	$\mathcal{O}(1/\varepsilon_2)$
h_5	10102	$\mathcal{O}(1/\varepsilon_1)$
h_6	8249	$\mathcal{O}(1/\varepsilon_1)$
h_{7a}	4993	$\mathcal{O}(1/\varepsilon_1)$
h_{7b}	1996	$\mathcal{O}(1)$
h_{7c}	688	$\mathcal{O}(1)$
h_8	5642	$\mathcal{O}(1/\varepsilon_1)$
d_{1a}	523	$\mathcal{O}(1)$
d_{1b}	179	$\mathcal{O}(1)$
d_{1c}	331	$\mathcal{O}(1)$

$$
\begin{aligned}
\frac{dT_m}{dt} &= \frac{[F_{tf}(T_{tf}-T_{\text{ref}})]_s}{V_m}\left(\frac{u_{cp}-k_m u_m}{\varepsilon_1}+u_{tf}+k_{hf}u_{hf}+k_{tr}u_{tr}\right)\\
\frac{dT_c}{dt} &= \frac{[F_{tf}(T_{tf}-T_{\text{ref}})]_s}{V_c}\left(\frac{u_{q\text{rec}}-k_c u_c}{\varepsilon_2}+\frac{k_m u_m}{\varepsilon_1}\right)\\
\frac{dT_f}{dt} &= \frac{[F_{tf}(T_{tf}-T_{\text{ref}})]_s}{V_f}\left(\frac{k_c u_c-k_f u_f}{\varepsilon_2}+k_{qf}u_{qf}\right)\\
\frac{dT_r}{dt} &= \frac{[F_{tf}(T_{tf}-T_{\text{ref}})]_s}{V_r}\left(\frac{k_f u_f-k_r u_r}{\varepsilon_2}-k_{hr}u_{hr}\right)\\
\frac{dT_h}{dt} &= \frac{[F_{tf}(T_{tf}-T_{\text{ref}})]_s}{V_h}\left(\frac{k_r u_r-u_{q\text{rec}}}{\varepsilon_2}-\frac{k_h u_h}{\varepsilon_1}\right)\\
\frac{dT_{cl}}{dt} &= \frac{[F_{tf}(T_{tf}-T_{\text{ref}})]_s}{V_{cl}}\left(\frac{k_h u_h-k_{cl}u_{cl}}{\varepsilon_1}-k_{cl}u_{cl}\right)\\
\frac{dT_{sp}}{dt} &= \frac{[F_{tf}(T_{tf}-T_{\text{ref}})]_s}{V_{sp}}\left(\frac{k_{cl}u_{cl}-k_{sp}u_{sp}}{\varepsilon_1}-k_P u_P-k_l u_l\right)\\
\frac{dT_{cp}}{dt} &= \frac{[F_{tf}(T_{tf}-T_{\text{ref}})]_s}{V_{cp}}\left(\frac{k_{sp}u_{sp}-u_{cp}}{\varepsilon_1}+k_w u_w\right)
\end{aligned}
\tag{3}
$$

or, equivalently, in a vector form

$$
\frac{d\mathbf{T}}{dt}=\sum_{i=0}^{2}\frac{1}{\varepsilon_i}\mathbf{F}_i\mathbf{g}_i \tag{4}
$$

with

$$
\mathbf{T}=[T_m,T_c,T_f,T_r,T_h,T_{cl},T_s,T_{cp}]^T
$$

$$
\mathbf{F}_0=\begin{bmatrix}1 & & \mathbf{0}_{1\times5}\\ & \mathbf{0}_{1\times6} & \\ \mathbf{0}_{2\times1} & \mathbf{I}_{2\times2} & \mathbf{0}_{2\times3}\\ & \mathbf{0}_{1\times6} & \\ \mathbf{0}_{3\times3} & & \mathbf{I}_{3\times3}\end{bmatrix}
$$

$$
\mathbf{g}_0=[F_{tf}(T_{tf}-T_{\text{ref}})]_s\begin{bmatrix}\frac{u_{tf}+k_{hf}u_{hf}+k_{tr}u_{tr}}{V_m}\\ \frac{k_{qf}u_{qf}}{V_f}\\ -\frac{k_{hr}u_{hr}}{V_r}\\ -\frac{k_{qcl}u_{qcl}}{V_{cl}}\\ \frac{-k_P u_P-k_l u_l}{V_{sp}}\\ \frac{k_w u_w}{V_{cp}}\end{bmatrix}
$$

$$
\mathbf{F}_1=\begin{bmatrix}\mathbf{I}_{2\times2} & \mathbf{0}_{2\times4}\\ \mathbf{0}_{2\times6} & \\ \mathbf{0}_{4\times2} & \mathbf{I}_{4\times4}\end{bmatrix}
$$

$$
\mathbf{g}_1=[F_{tf}(T_{tf}-T_{\text{ref}})]_s\begin{bmatrix}\frac{u_{cp}-k_m u_m}{Vm}\\ \frac{k_m u_m}{V_c}\\ -\frac{k_h u_h}{V_h}\\ \frac{k_h u_h-k_{cl}u_{cl}}{V_{cl}}\\ \frac{k_{cl}u_{cl}-k_{sp}u_{sp}}{V_{sp}}\\ \frac{k_{sp}u_{sp}-u_{cp}}{V_{cp}}\end{bmatrix}
$$

$$
\mathbf{F}_2=\begin{bmatrix}\mathbf{0}_{1\times4}\\ \mathbf{I}_{4\times4}\\ \mathbf{0}_{3\times4}\end{bmatrix}
$$

$$
\mathbf{g}_2=[F_{tf}(T_{tf}-T_{\text{ref}})]_s\begin{bmatrix}\frac{u_{q\text{rec}}-k_c u_c}{V_c}\\ \frac{k_c u_c-k_f u_f}{V_f}\\ \frac{k_f u_f-k_r u_r}{V_r}\\ \frac{k_r u_r-u_{q\text{rec}}}{V_h}\end{bmatrix}
$$

where $\mathbf{I}$ is the identity matrix, and $\mathbf{0}$ is a matrix with all entries equal to 0.

Note that Eq. 4 suggests possibly three-time scale energy dynamics. We follow a sequential application of singular perturbations for deriving approximate models in each time scale.

Let us define the fast time scale $\tau_2=t/\varepsilon_2$. Substituting this into Eq. 3 and taking the limit $\varepsilon_2\to0$, we obtain the description of the energy dynamics in the fast time scale

$$
\frac{d\mathbf{T}}{d\tau_2}=\mathbf{F}_2\mathbf{g}_2 \tag{5}
$$

We note that only the temperatures of the FEHE, the furnace and the reactor evolve in the fast time scale (i.e., $\mathbf{T}_2=\{T_c,T_f,T_r,T_h\}$). From Eq. 5, we identify the quasi-steady state constraints, $\mathbf{g}_2=0$, and it can be verified that these equations are not linearly independent. Thus, we take a linearly independent subset $\tilde{\mathbf{g}}_2$, which is defined by $\mathbf{g}_2=\mathbf{B}_2\tilde{\mathbf{g}}_2$, with

$$
\mathbf{B}_2=[F_{tf}(T_{tf}-T_{\text{ref}})]_s\begin{bmatrix}1/V_c & 0 & 0\\ 0 & 1/V_f & 0\\ 0 & 0 & 1/V_r\\ -1/V_h & -1/V_h & -1/V_h\end{bmatrix}
$$

$$
\tilde{\mathbf{g}}_2=\begin{bmatrix}u_{q\text{rec}}-k_c u_c\\ k_c u_c-k_f u_f\\ k_f u_f-k_r u_r\end{bmatrix}
$$

Now, we take the same limit $\varepsilon_2\to0$ in the slow time scale t, and obtain

$$\frac{d\mathbf{T}}{dt}=\sum_{i=0}^{1}\frac{1}{\varepsilon_i}\mathbf{F}_i\mathbf{g}_i+\mathbf{F}_2\mathbf{B}_2\left(\lim_{\varepsilon_2\to 0}\frac{\tilde{\mathbf{g}}_2}{\varepsilon_2}\right)$$
$$0=\tilde{\mathbf{g}}_2$$

which describes the energy dynamics after the fast boundary layer. The limiting terms represent the differences between the large energy flows, which are indeterminate yet finite. These terms can be represented by a set of algebraic variables $\mathbf{z}_2$ to obtain the following DAE system

$$\frac{d\mathbf{T}}{dt}=\sum_{i=0}^{1}\frac{1}{\varepsilon_i}\mathbf{F}_i\mathbf{g}_i+\mathbf{F}_2\mathbf{B}_2\mathbf{z}_2 \qquad (6)$$
$$0=\tilde{\mathbf{g}}_2$$

The algebraic variables $\mathbf{z}_2$ can be evaluated by differentiating the constraints in Eq. 6

$$\mathbf{z}_2=-\left(\mathcal{L}_{\mathbf{F}_2\mathbf{B}_2}\tilde{\mathbf{g}}_2\right)^{-1}\left[\sum_{i=0}^{1}\frac{1}{\varepsilon_i}\mathcal{L}_{\mathbf{F}_i\mathbf{g}_i}\tilde{\mathbf{g}}_2\right] \qquad (7)$$

where $\mathcal{L}$ represents the Lie derivative, which is defined as

$$\mathcal{L}_{\mathbf{f}(\mathbf{x})}\mathbf{h}(\mathbf{x})=\mathbf{J_h}\mathbf{f}$$

where $\mathbf{h}(\mathbf{x})$ is a vector, $\mathbf{f}(\mathbf{x})$ is a vector (or a matrix), and $\mathbf{J_h}=\left\{\frac{\partial h_i}{\partial x_j}\right\}$ is the jacobian matrix of $\mathbf{h}$.

Using the solution for $\mathbf{z}_2$ in Eq. 7, we can rewrite Eq. 6 as follows

$$\frac{d\mathbf{T}}{dt}=\sum_{i=0}^{1}\frac{1}{\varepsilon_i}\mathbf{F}_i\mathbf{g}_i-\mathbf{F}_2\mathbf{B}_2\left(\mathcal{L}_{\mathbf{F}_2\mathbf{B}_2}\tilde{\mathbf{g}}_2\right)^{-1}\left[\sum_{i=0}^{1}\frac{1}{\varepsilon_i}\mathcal{L}_{\mathbf{F}_i\mathbf{g}_i}\tilde{\mathbf{g}}_2\right] \qquad (8)$$
$$0=\tilde{\mathbf{g}}_2$$

or, in a slightly rearranged form

$$\frac{d\mathbf{T}}{dt}=\sum_{i=0}^{1}\frac{1}{\varepsilon_i}\hat{\mathbf{F}}_i\hat{\mathbf{g}}_i \qquad (9)$$
$$0=\tilde{\mathbf{g}}_2$$

where $\hat{\mathbf{F}}_i$ and $\hat{\mathbf{g}}_i$ represent the correspondingly adjusted selector matrices and vectors, respectively, given as

$$\hat{\mathbf{F}}_0=\begin{bmatrix}1 & & \mathbf{0}_{1\times 5}\\ \mathbf{0}_{3\times 1} & \mathbf{1}_{3\times 1} & \mathbf{0}_{3\times 4}\\ \mathbf{0}_{4\times 2} & & \mathbf{I}_{4\times 4}\end{bmatrix}$$

$$\hat{\mathbf{g}}_0=\left[F_{tf}(T_{tf}-T_{\mathrm{ref}})\right]_s$$

$$\times\begin{bmatrix}\frac{u_{tf}+k_{hf}u_{hf}+k_{tr}u_{tr}}{V_m}\\ \frac{k_{qf}u_{qf}-k_{hr}u_{hr}-\frac{V_h}{V_m}(k_{hf}u_{hf}+k_{tr}u_{tr}+u_{tf})}{V_c+V_f+V_r+\frac{8F\rho C_p}{UA}V_h}\\ \frac{\frac{V_c+V_f+V_r}{V_m}(k_{hf}u_{hf}+k_{tr}u_{tr}+u_{tf})+\frac{8F\rho C_p}{UA}(k_{qf}u_{qf}-k_{hr}u_{hr})}{V_c+V_f+V_r+\frac{8F\rho C_p}{UA}V_h}\\ -\frac{k_{qcl}u_{qcl}}{V_{cl}}\\ \frac{-k_Pu_P-k_lu_l}{V_{sp}}\\ \frac{k_wu_w}{V_{cp}}\end{bmatrix}$$

$$\hat{\mathbf{F}}_1=\begin{bmatrix}1 & & \mathbf{0}_{1\times 5}\\ \mathbf{0}_{3\times 1} & \mathbf{1}_{3\times 1} & \mathbf{0}_{3\times 4}\\ \mathbf{0}_{4\times 2} & & \mathbf{I}_{4\times 4}\end{bmatrix}$$

$$\hat{\mathbf{g}}_1=\left[F_{tf}(T_{tf}-T_{ref})\right]_s$$

$$\times\begin{bmatrix}\frac{u_{cp}-k_mu_m}{Vm}\\ \frac{k_mu_m-k_hu_h+\frac{V_h}{V_m}(k_mu_m-u_{cp})}{V_c+V_f+V_r+\frac{8F\rho C_p}{UA}V_h}\\ \frac{\frac{V_c+V_f+V_r}{V_m}(u_{cp}-k_mu_m)+\frac{8F\rho C_p}{UA}(k_mu_m-k_hu_h)}{V_c+V_f+V_r+\frac{8F\rho C_p}{UA}V_h}\\ \frac{k_hu_h-k_{cl}u_{cl}}{V_{cl}}\\ \frac{k_{cl}u_{cl}-k_{sp}u_{sp}}{V_{sp}}\\ \frac{k_{sp}u_{sp}-u_{cp}}{V_{cp}}\end{bmatrix}$$

where $\mathbf{1}$ is a matrix with all entries equal to 1.

Note that the dynamic equations after the fast boundary layer (i.e., Eq. 9) are also in a singularly perturbed form, indicating that further model reduction can be performed.

Let us define an intermediate time scale $\tau_1=t/\varepsilon_1$. Substituting this into Eq. 9 and taking the limit $\varepsilon_1\to 0$, we obtain the description of the intermediate energy dynamics

$$\frac{d\mathbf{T}}{d\tau_1}=\hat{\mathbf{F}}_1\hat{\mathbf{g}}_1 \qquad (10)$$
$$0=\tilde{\mathbf{g}}_2$$

Note that all the temperatures evolve in this time scale. The quasi-steady state constraints of the intermediate time scale dynamics are identified as $\hat{\mathbf{g}}_1=0$, which are linearly dependent. A linearly independent subset $\tilde{\hat{\mathbf{g}}}_1$, defined as $\hat{\mathbf{g}}_1=\mathbf{B}_1\tilde{\hat{\mathbf{g}}}_1$, is taken, with

$$\mathbf{B}_1=\left[F_{tf}(T_{tf}-T_{\mathrm{ref}})\right]_s$$

$$\times\begin{bmatrix}\frac{1}{V_m} & 0 & 0 & 0\\ -\frac{\frac{V_h}{V_m}}{V_c+V_f+V_r+\frac{8\rho C_p}{UA}V_h} & \frac{1}{V_c+V_f+V_r+\frac{8\rho C_p}{UA}V_h} & 0 & 0\\ \frac{\frac{V_c+V_f+V_r}{V_m}}{V_c+V_f+V_r+\frac{8\rho C_p}{UA}V_h} & \frac{\frac{8F\rho C_p}{UA}}{V_c+V_f+V_r+\frac{8\rho C_p}{UA}V_h} & 0 & 0\\ 0 & 0 & \frac{1}{V_{cl}} & 0\\ 0 & 0 & 0 & \frac{1}{V_{sp}}\\ -\frac{1}{V_{cp}} & -\frac{1}{V_{cp}} & -\frac{1}{V_{cp}} & -\frac{1}{V_{cp}}\end{bmatrix}$$

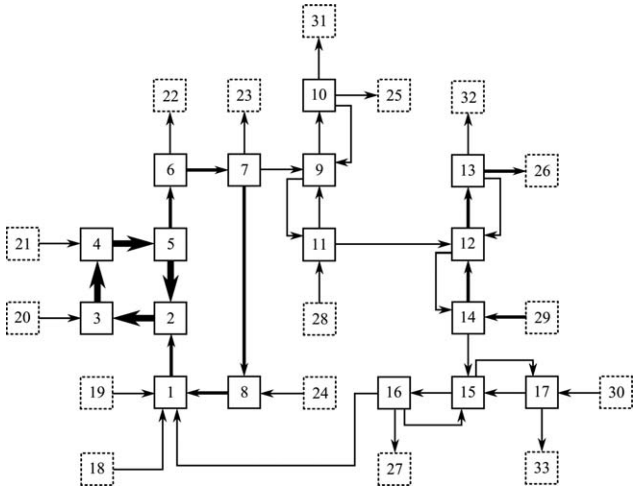

Figure 4. Energy flow graph of the HDA process.

$$\tilde{\hat{\mathbf{g}}}_1 = \begin{bmatrix} u_{cp} - k_m u_m \\ k_m u_m - k_h u_h \\ k_h u_h - k_{cl} u_{cl} \\ k_{cl} u_{cl} - k_{sp} u_{sp} \end{bmatrix}$$

We take the same limit $\varepsilon_1 \to 0$ in the original time scale t, and obtain the description of the energy dynamics after the intermediate boundary layer

$$\begin{aligned} \frac{d\mathbf{T}}{dt} &= \hat{\mathbf{F}}_0 \hat{\mathbf{g}}_0 + \hat{\mathbf{F}}_1 \mathbf{B}_1 \left(\lim_{\varepsilon_1 \to 0} \frac{\tilde{\tilde{\mathbf{g}}}_1}{\varepsilon_1} \right) \\ 0 &= \tilde{\mathbf{g}}_2 \\ 0 &= \tilde{\tilde{\mathbf{g}}}_1 \end{aligned}$$

We define another set of algebraic variables $\mathbf{z}_1$ to represent the limiting terms, and obtain

$$\begin{aligned} \frac{d\mathbf{T}}{dt} &= \hat{\mathbf{F}}_0 \hat{\mathbf{g}}_0 + \hat{\mathbf{F}}_1 \mathbf{B}_1 \mathbf{z}_1 \\ 0 &= \tilde{\mathbf{g}}_2 \\ 0 &= \tilde{\tilde{\mathbf{g}}}_1 \end{aligned} \tag{11}$$

$\mathbf{z}_1$ can be computed by differentiating the constraints in Eq. 11

$$\mathbf{z}_1 = -(\mathcal{L}_{\hat{\mathbf{F}}_1 \mathbf{B}_1} \tilde{\tilde{\mathbf{g}}}_1)^{-1} (\mathcal{L}_{\hat{\mathbf{F}}_0 \hat{\mathbf{g}}_0} \tilde{\tilde{\mathbf{g}}}_1) \tag{12}$$

Using the solution of Eq. 12, the description of the slow energy dynamics is obtained

$$\begin{aligned} \frac{d\mathbf{T}}{dt} &= \hat{\mathbf{F}}_0 \hat{\mathbf{g}}_0 - \hat{\mathbf{F}}_1 \mathbf{B}_1 (\mathcal{L}_{\hat{\mathbf{F}}_1 \mathbf{B}_1} \tilde{\tilde{\mathbf{g}}}_1)^{-1} (\mathcal{L}_{\hat{\mathbf{F}}_0 \hat{\mathbf{g}}_0} \tilde{\tilde{\mathbf{g}}}_1) \\ 0 &= \tilde{\mathbf{g}}_2 \\ 0 &= \tilde{\tilde{\mathbf{g}}}_1 \end{aligned} \tag{13}$$

or in a rearranged form

$$\begin{aligned} \frac{d\mathbf{T}}{dt} &= \mathbf{F}_0' \mathbf{g}_0' \\ 0 &= \tilde{\mathbf{g}}_2 \\ 0 &= \tilde{\tilde{\mathbf{g}}}_1 \end{aligned} \tag{14}$$

where $\mathbf{F}_0'$ and $\mathbf{g}_0'$ are the correspondingly adjusted selector matrix and vector, respectively. The exact forms of $\mathbf{F}_0'$ and $\mathbf{g}_0'$ are not presented here for brevity.

Table 2. Node List of the HDA Energy Flow Graph

Normal Nodes		Auxiliary Nodes	
Index	Unit	Index	Unit
1	Mixer	18	Toluene feed stream
2	FEHE-Cold	19	H_2 feed stream
3	Furnace	20	Furnace source
4	Plug-flow reactor	21	Heat of reaction
5	FEHE-Hot	22	Cooler sink
6	Cooler	23	Purge stream
7	Separator	24	Compressor power input
8	Compressor	25	S-Condenser sink
9	Stabilizer (S)	26	P-Condenser sink
10	S-Condenser	27	R-Condenser sink
11	S-Reboiler	28	S-Reboiler source
12	Product column (P)	29	P-Reboiler source
13	P-Condenser	30	R-Reboiler source
14	P-Reboiler	31	Methane product stream
15	Recycle column (R)	32	Benzene product stream
16	R-Condenser	33	Diphenyl product stream
17	R-Reboiler		

In summary, the energy dynamics of the FEHE, the furnace and the reactor evolve over all three time scales, whereas those of the mixer, the cooler, the separator, and the compressor evolve in the intermediate and slow time scales.

Graph-Theoretic Analysis. Let us now proceed to the graph-theoretic analysis. The HDA process network can be represented as an energy flow graph $\mathcal{G}$, as shown in Figure 4. The node list is provided in Table 2. The graph reduction framework is applied to the network using the information in Figure 4 and Table 1 to obtain the following results.

The subgraph corresponding to the fast time scale $\mathcal{H}_2$, with the largest magnitude $\mathcal{O}(1/\varepsilon_2)$ flows, is shown in Figure 5a. The units evolving in this time scale are the nodes of

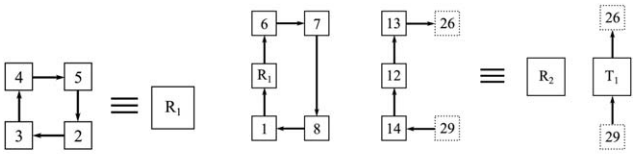

(a) with the largest energy flows (b) with the intermediate energy flows

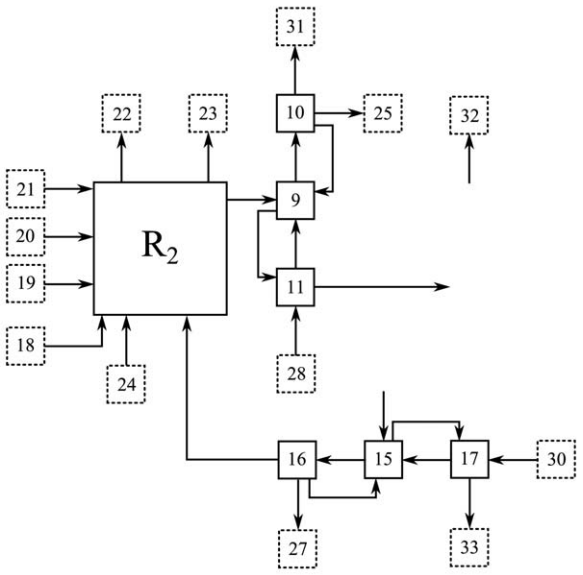

(c) with the smallest energy flows

Figure 5. Subgraphs of the HDA reaction part energy flow graph.

$\mathcal{H}_2$, that is, $\mathcal{T}_2=\{2,3,4,5\}$. This subgraph contains a prototype recycle, which can be simplified as a single composite node R_1. Figure 5b shows the subgraph for the intermediate time scale $\mathcal{H}_1$. A subset of the units which evolve in this time scale are given by $\mathcal{T}_1=\{1,R_1,6,7,8,12,13,14\}$. This subgraph has one prototype recycle which can be clustered to form a composite node R_2. Also, a prototype throughput is identified, which is simplified as a single composite node T_1, and it is removed from the original energy flow graph $\mathcal{G}$. Lastly, the slow time scale subgraph $\mathcal{H}_0$ is shown in Figure 5c. The units evolving in this time scale are given as $\mathcal{T}_0=\{R_2,9,10,11,15,16,17\}$.

We conclude that, based on the result above, the network is expected to exhibit three-time scale energy dynamics, and the time scales wherein each unit evolves are summarized in Table 3. Note that this result matches the outcome of the detailed mathematical analysis.

The full order dynamic model equations are obtained as

$$\frac{d\mathbf{H}}{dt}=\frac{1}{\varepsilon_0}\mathbf{g}_0+\frac{1}{\varepsilon_1}\mathbf{g}_1+\frac{1}{\varepsilon_2}\mathbf{g}_2 \tag{15}$$

with

$$\mathbf{g}_0=h_{18-1,s}\begin{bmatrix} k_{18-1}u_{18-1}+k_{19-1}u_{19-1}+k_{16-1}u_{16-1}\\ 0\\ k_{20-3}u_{20-3}\\ k_{21-4}u_{21-4}\\ 0\\ -k_{6-22}u_{6-22}\\ -k_{7-9}u_{7-9}-k_{7-23}u_{7-23}\\ k_{24-8}u_{24-8}\end{bmatrix}$$

$$\mathbf{g}_1=h_{18-1,s}\begin{bmatrix} -k_{1-2}u_{1-2}+k_{8-1}u_{8-1}\\ k_{1-2}u_{1-2}\\ 0\\ 0\\ -k_{5-6}u_{5-6}\\ k_{5-6}u_{5-6}-k_{6-7}u_{6-7}\\ k_{6-7}u_{6-7}-k_{7-8}u_{7-8}\\ k_{7-8}u_{7-8}-k_{8-1}u_{8-1}\end{bmatrix}$$

$$\mathbf{g}_2=h_{18-1,s}\begin{bmatrix} 0\\ -k_{2-3}u_{2-3}+k_{5-2}u_{5-2}\\ k_{2-3}u_{2-3}-k_{3-4}u_{3-4}\\ k_{3-4}u_{3-4}-k_{4-5}u_{4-5}\\ k_{4-5}u_{4-5}-k_{5-2}u_{5-2}\\ 0\\ 0\\ 0\end{bmatrix}$$

where h_{i-j} represents the energy flow from the i-th node to the j-th node. Note that Eq. 15 has the same canonical form as Eq. 4.

Table 3. Summary of Time Scale Analysis for the HDA Process

	Evolution in Each Time Scale		
Enthalpy	Fast	Intermediate	Slow
H_1	X	O	O
H_2	O	O	O
H_3	O	O	O
H_4	O	O	O
H_5	O	O	O
H_6	X	O	O
H_7	X	O	O
H_8	X	O	O
H_9	X	X	O
H_{10}	X	X	O
H_{11}	X	X	O
H_{12}	X	O	X
H_{13}	X	O	X
H_{14}	X	O	X
H_{15}	X	X	O
H_{16}	X	X	O
H_{17}	X	X	O

The dynamics of the reduced order model for the fast time scale is given as

$$\frac{d\mathbf{H}_2}{d\tau_2}=\mathbf{g}_2^{'} \tag{16}$$

with

$$\mathbf{g}_2^{'}=h_{18-1,s}\begin{bmatrix} -k_{2-3}u_{2-3}+k_{5-2}u_{5-2}\\ k_{2-3}u_{2-3}-k_{3-4}u_{3-4}\\ k_{3-4}u_{3-4}-k_{4-5}u_{4-5}\\ k_{4-5}u_{4-5}-k_{5-2}u_{5-2}\end{bmatrix}$$

where $\mathbf{H}_2=\{H_2,H_3,H_4,H_5\}$. The quasi-steady state constraints, which are not lineary independent, are given as $\mathbf{g}_2^{'}=0$. Note that, by premultiplying Eq. 5 by $\mathbf{F}_2^T$, we can rewrite Eq. 5 so that it is in the same canonical form with Eq. 16.

The intermediate time scale dynamics is given as

$$\begin{aligned}\frac{d\mathbf{H}_1}{d\tau_1}&=\mathbf{g}_1+\mathbf{C}_2\mathbf{B}_2\bar{\mathbf{z}}_2\\ 0&=\tilde{\mathbf{g}}_2^{'}\end{aligned} \tag{17}$$

with

$$\mathbf{B}_2=\begin{bmatrix}\mathbf{I}_{3\times3}\\ -\mathbf{1}_{1\times3}\end{bmatrix}$$

$$\mathbf{C}_2=\begin{bmatrix}\mathbf{0}_{1\times4}\\ \mathbf{I}_{4\times4}\\ \mathbf{0}_{3\times3}\end{bmatrix}$$

where $\mathbf{H}_1=\{H_1,H_2,\ldots,H_8\}$. $\tilde{\mathbf{g}}_2^{'}$, which represents a linearly independent subset of the quasi-steady state constraints, is given as $\mathbf{g}_2^{'}=\mathbf{B}_2\tilde{\mathbf{g}}_2^{'}$. $\bar{\mathbf{z}}_2$ is a vector of algebraic variables, given as $\lim_{\varepsilon_2\to0}\tilde{\mathbf{g}}_2^{'}/\varepsilon_2$. The linearly dependent quasi-steady state constraints of the intermediate energy dynamics, $\mathbf{g}_1^{'}=\mathbf{g}_1+\mathbf{C}_2\mathbf{B}_2\bar{\mathbf{z}}_2=0$, are also given by the algorithm. It can be shown that Eq. 17 has the same canonical form with Eq. 6.

Table 4. Summary of the Hierarchical Control Structure for the HDA Process

Time Scale	Controlled Output	Manipulated Input
Fast	T_5	h_{5-2}
Intermediate	T_6	h_{6-22}
Slow	T_3	h_{20-3}

Finally, the slow time scale dynamic model is given as

$$\begin{aligned}\frac{d\mathbf{H}}{dt}&=\mathbf{g}_0+\mathbf{C}_1\mathbf{B}_1\bar{\mathbf{z}}_1\\ 0&=\tilde{\mathbf{g}}_2'\\ 0&=\tilde{\mathbf{g}}_1'\end{aligned}\tag{18}$$

with

$$\mathbf{B}_1=\begin{bmatrix}\mathbf{I}_{7\times7}\\ -\mathbf{1}_{1\times7}\end{bmatrix}$$

$$\mathbf{C}_1=\mathbf{I}_{8\times8}$$

The linearly independent subset of the quasi-steady state constraints $\tilde{\mathbf{g}}_1'$ can be defined similarly as is done in the intermediate time scale dynamics, and $\bar{\mathbf{z}}_1$ are algebraic variables, defined by $\lim_{\varepsilon_1\to0}\tilde{\mathbf{g}}_1'/\varepsilon_1$. Note that Eq. 18 has the same canonical form with Eq. 11.

Finally, the controlled outputs and the potential manipulated inputs available in each time scale are obtained using the algorithm. In the fast time scale (τ_2), the enthalpies of the FEHE, the furnace, and the reactor need to be controlled (i.e., $\mathcal{Y}(\tau_2)=\{2,3,4,5\}$), and all but one out of four units can be controlled simultaneously, noting that $\mathcal{H}_2$ contains no auxiliary node. Potential manipulated inputs in this time scale include: $\mathcal{U}(\tau_2)=\{2\text{-}3, 3\text{-}4, 4\text{-}5, 5\text{-}2\}$.

The enthalpies of the mixer, the cooler, the separator, and the compressor as well as the total enthalpy of the FEHE-reactor recycle loop need to be controlled in the intermediate time scale (i.e., $\mathcal{Y}(\tau_1)=\{1,R_1,6,7,8\}$), and all but one out of five can be controlled independently since, in $\mathcal{H}_1$, R_2 does not have any auxiliary node connected to it. The following set of potential manipulated inputs is given: $\mathcal{U}(\tau_1)=\{1\text{-}2, 6\text{-}7, 7\text{-}8, 8\text{-}1, 5\text{-}6\}$. Lastly, the total network enthalpy needs to be controlled in the slow time scale, and this can be achieved using any small external flow.

Based on this information, a hierarchical control strategy can be used to control the energy dynamics of the network.

Table 5. Nominal Values of the State Variables and the Process Parameters

Parameter	Value	Parameter	Value
F_{TF}	0.0033 m^3/s	F_{HF}	0.0356 m^3/s
F_{TR}	9.7×10^{-4} m^3/s	F_q	0.0034 m^3/s
R	0.3087 m^3/s	UA	8.24×10^5 W/K
V_m	0.1 m^3	V_C	14.16 m^3
V_f	8.5 m^3	V_R	110 m^3
V_H	14.16 m^3	V_{cl}	8.5 m^3
V_s	8.5 m^3	V_{cp}	8.5 m^3
T_{TF}	303 K	T_{HF}	303 K
T_{TR}	457 K	$T_{m,s}$	343.91 K
$T_{C,s}$	881.11 K	$T_{f,s}$	896.03 K
$T_{R,s}$	940.60 K	$T_{q,s}$	895.99 K
$T_{H,s}$	384.45 K	$T_{cl,s}$	317.55 K
$T_{s,s}$	317.55 K	$T_{cp,s}$	348.71 K

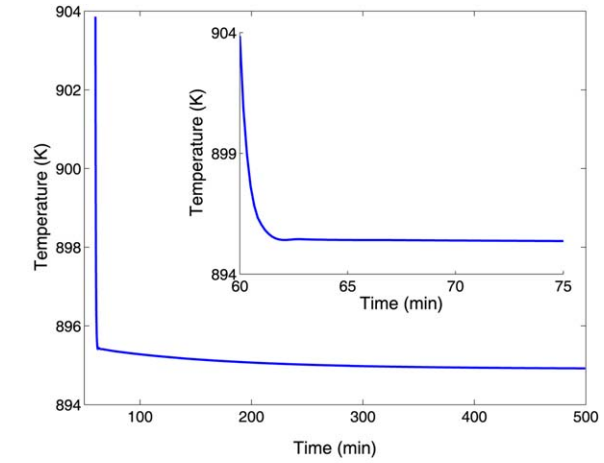

(a) Overall

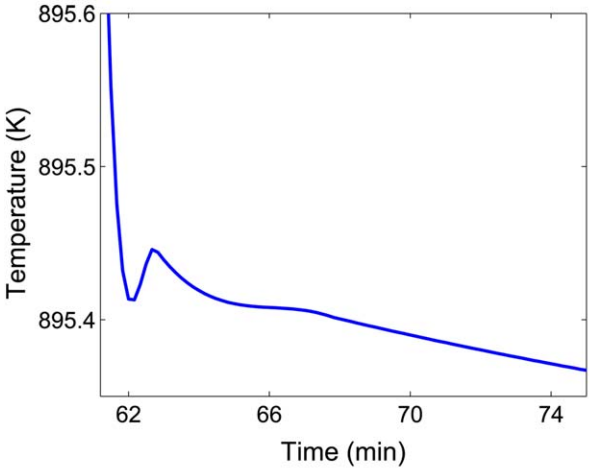

(b) Intermediate

Figure 6. Evolution of the furnace temperature.

[Color figure can be viewed in the online issue, which is available at wileyonlinelibrary.com.]

For example, it was shown that the energy dynamics of the HDA network can be controlled using simple PI controllers,[19] addressing different control objectives in different time scales as summarized in Table 4. Also, the reduced

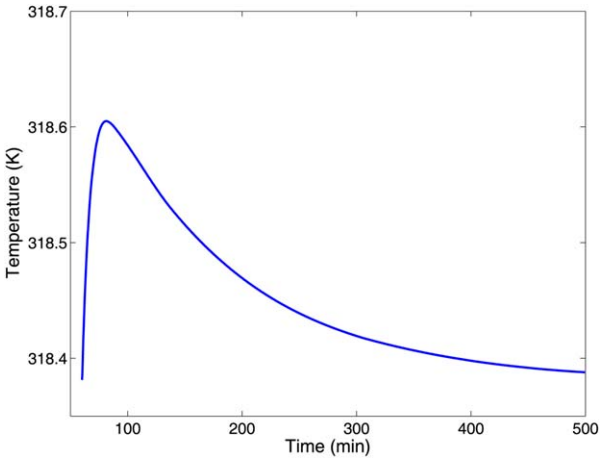

Figure 7. Evolution of the separator temperature.

[Color figure can be viewed in the online issue, which is available at wileyonlinelibrary.com.]

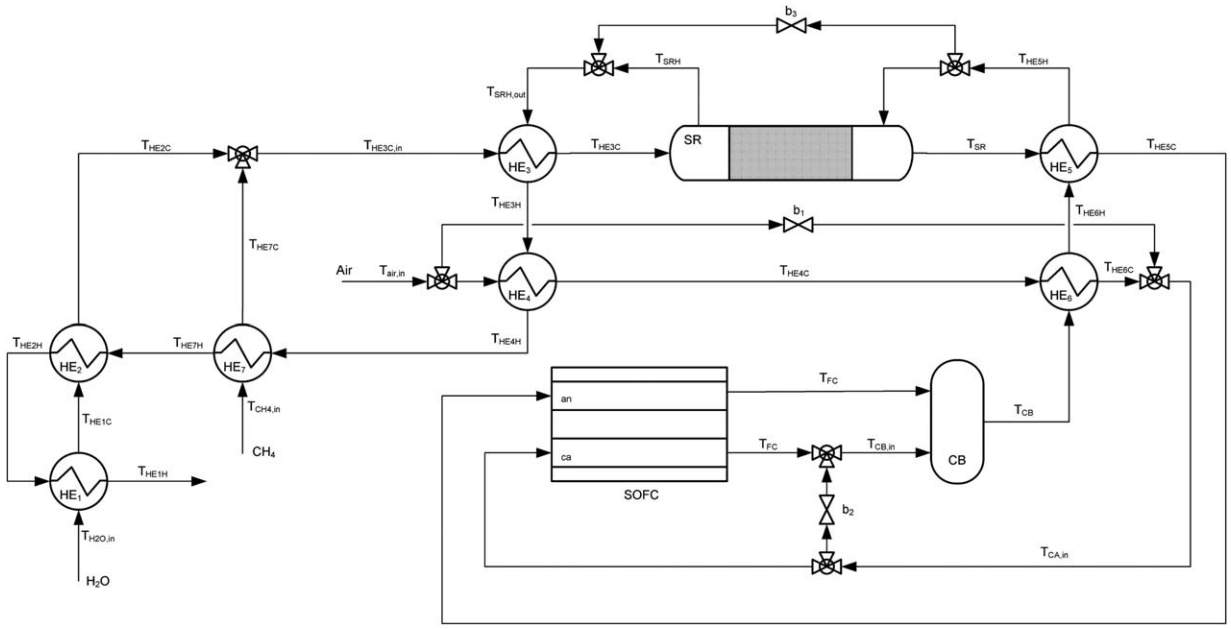

Figure 8. Energy-integrated SOFC system.

models derived above can be used to design nonlinear model-based controllers.

Simulation Study. To further validate the results obtained using the graph-theoretic framework, we now perform numerical simulations using the equations in 2, along with the equations of the material dynamics. For simplicity, we assume that there is no phase change in the FEHE, and the holdups of all units are constant. Also, we assume constant heat capacity and density. Reaction rates are computed using the expressions provided in the Ref. 20. The nominal values of the state variables and the process parameters are given in Table 5.

We consider the open-loop responses of the system by increasing the temperature of the furnace by 1%. Figure 6 shows the evolution of the furnace temperature. We note that the furnace temperature quickly drops and then slowly goes back to the steady state. Also, an intermediate time scale dynamics is observed as shown in Figure 6b. The separator temperature increases in a slower time scale compared to the furnace, and then returns slowly to the steady state, as shown in Figure 7, indicating that it evolves in the intermediate and the slow time scales. Note that the simulation results are consistent with the results obtained using either the detailed mathematical analysis or the graph-theoretic framework.

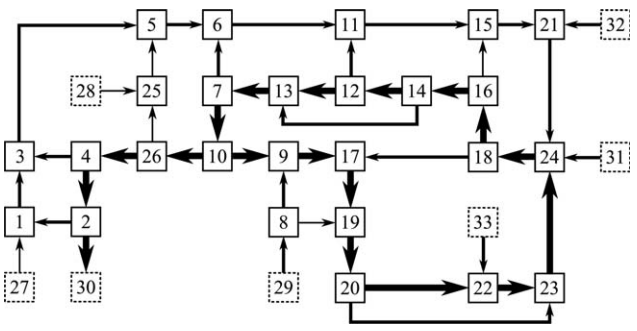

Figure 9. Energy flow graph of the energy-integrated SOFC system.

Energy-integrated solid oxide fuel cell system

Let us now consider an energy-integrated solid oxide fuel cell (SOFC) system with an external reformer,[21] as shown in Figure 8. In this network, both the outlet streams of the SOFC are fed to a catalytic burner to achieve complete combustion of methane, carbon monoxide, and unreacted hydrogen. Then, the outlet stream of the burner, which is at high temperature, provides energy to the reformer, where endothermic reactions occur, and the feed streams, resulting in a tightly integrated configuration. The energy flow graph of the network is shown in Figure 9, and all the nodes are listed in Table 6. The various energy flows of the network span a wide range of values from 0.256 to 49.098 kW. The orders of magnitude of the energy flows are determined following a similar procedure used in the previous example, as summarized in Table 7. ε_1 and ε_2 are small parameters

Table 6. Node List of the Energy-Integrated SOFC System

Index	Unit	Index	Unit
Normal Nodes			
1	HE1-Cold	14	Splitter 2
2	HE1-Hot	15	HE5-Cold
3	HE2-Cold	16	HE5-Hot
4	HE2-Hot	17	HE6-Cold
5	Mixer 1	18	HE6-Hot
6	HE3-Cold	19	Mixer 3
7	HE3-Hot	20	Splitter 3
8	Splitter 1	21	SOFC anode
9	HE4-Cold	22	SOFC cathode
10	HE4-Hot	23	Mixer 4
11	Steam reformer (SR)	24	Catalytic burner (CB)
12	SR jacket	25	HE7-Cold
13	Mixer 2	26	HE7-Hot
Auxiliary Nodes			
27	Water feed stream	31	CB energy input
28	Methane feed stream	32	SOFC anode heat of reaction
29	Air feed stream	33	SOFC cathode heat of reaction
30	HE1 sink		

Table 7. Summary of Orders of Magnitude of the Energy Flows of the Energy-Integrated SOFC System

Energy Flow	mC_pT(kW)	Order of Magnitude	Energy Flow	mC_pT(kW)	Order of Magnitude
28 → 25	0.256	$\mathcal{O}(1)$	17 → 19	27.751	$\mathcal{O}(1/\varepsilon_2)$
25 → 5	0.447	$\mathcal{O}(1)$	19 → 20	28.627	$\mathcal{O}(1/\varepsilon_2)$
27 → 1	1.049	$\mathcal{O}(1/\varepsilon_1)$	20 → 22	25.764	$\mathcal{O}(1/\varepsilon_2)$
1 → 3	1.313	$\mathcal{O}(1/\varepsilon_1)$	22 → 23	30.768	$\mathcal{O}(1/\varepsilon_2)$
3 → 5	1.815	$\mathcal{O}(1/\varepsilon_1)$	24 → 18	49.098	$\mathcal{O}(1/\varepsilon_2)$
5 → 6	2.450	$\mathcal{O}(1/\varepsilon_1)$	18 → 16	39.934	$\mathcal{O}(1/\varepsilon_2)$
6 → 11	3.901	$\mathcal{O}(1/\varepsilon_1)$	16 → 14	39.722	$\mathcal{O}(1/\varepsilon_2)$
11 → 15	4.997	$\mathcal{O}(1/\varepsilon_1)$	13 → 7	35.217	$\mathcal{O}(1/\varepsilon_2)$
15 → 21	5.215	$\mathcal{O}(1/\varepsilon_1)$	7 → 10	33.821	$\mathcal{O}(1/\varepsilon_2)$
21 → 24	6.231	$\mathcal{O}(1/\varepsilon_1)$	10 → 26	21.441	$\mathcal{O}(1/\varepsilon_2)$
29 → 8	8.768	$\mathcal{O}(1/\varepsilon_1)$	26 → 4	21.163	$\mathcal{O}(1/\varepsilon_2)$
8 → 9	7.891	$\mathcal{O}(1/\varepsilon_1)$	4 → 2	17.195	$\mathcal{O}(1/\varepsilon_2)$
9 → 17	19.303	$\mathcal{O}(1/\varepsilon_2)$	2 → 30	16.710	$\mathcal{O}(1/\varepsilon_2)$

($\varepsilon_2 \ll \varepsilon_1 \ll 1$), which are the ratios of the energy input through the methane feed to the energy input through the air feed and the energy of the catalytic burner outlet stream, respectively.

We apply the graph-theoretic reduction to the network using the information in Figure 9 and Table 7 as inputs. The graph-theoretic algorithm checks the *feasibility* of the network, based on the energy balance around all the normal nodes as well as the composite nodes. Specifically, the highest order of magnitude among the edges entering the node N should match with the highest order of magnitude among the edges leaving the node N to have a feasible energy flow structure around the unit N. In this case, the energy flow structure around the recycle, consisting of nodes 24-18-16-16-12-13-7-10-9-17-19-20-22-23, is infeasible as the recycle has an energy output of $\mathcal{O}(1/\varepsilon_2)$, but no energy input of $\mathcal{O}(1/\varepsilon_2)$. This infeasibility may originate from either inappropriately determined orders of magnitude or no clear segregation of energy flows. To determine which is the case, we remove the energy feasibility check and apply the algorithm again.

Figure 10a shows the subgraph corresponding to the fast time scale. The units evolving in this time scale are: $\mathcal{T}_2=\{2,4,7,9,10,12,13,14,16,17,18,19,20,22,23,24,26\}$. A prototype recycle is identified, and can be simplified as a single composite node R_1. Also, a prototype throughput is identified and clustered to form a composite node T_1. The composite node T_1 is then removed from the original energy flow graph. The subgraph of the intermediate time scale is shown in Figure 10b. A set of units evolving in this time scale is identified as: $\mathcal{T}_1=\{1,3,5,6,8,11,15,21\}$. Lastly, the slow time scale subgraph is shown in Figure 10c. The following unit evolves in this time scale: $\mathcal{T}_0=\{25\}$.

We note that the composite node R_1 has one energy output of $\mathcal{O}(1/\varepsilon_2)$ (i.e., 10–26) and several energy inputs of $\mathcal{O}(1/\varepsilon_1)$ (e.g., 33-22, 21–24). Although none of these energy inputs is of $\mathcal{O}(1/\varepsilon_2)$, the sum of the energy content of the inputs is comparable to the energy content of the flow 10–26, implying that there is no clear segregation of energy flows in the network.

We conclude that, despite the tight energy integration throughout the network, there is no process unit with

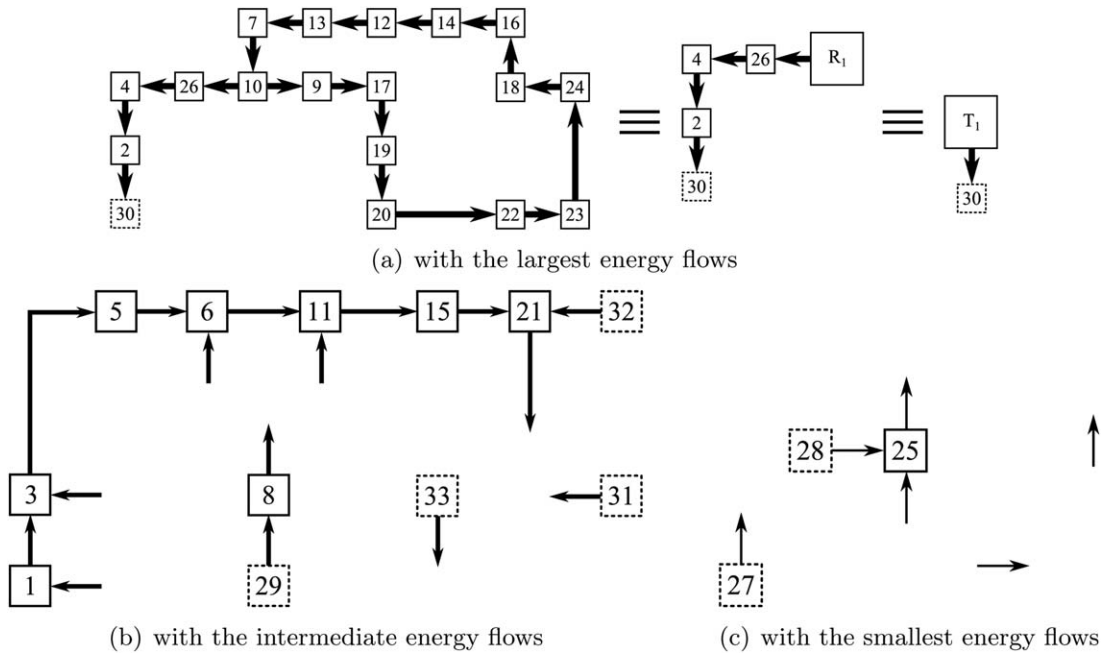

Figure 10. Subgraphs of the energy-integrated SOFC energy flow graph.

Table 8. Summary of Time Scale Analysis for the Energy-Integrated SOFC Process

	Evolution in Each Time Scale		
Enthalpy	Fast	Intermediate	Slow
H_1	X	O	X
H_2	O	X	X
H_3	X	O	X
H_4	O	X	X
H_5	X	O	X
H_6	X	O	X
H_7	O	X	X
H_8	X	O	X
H_9	O	X	X
H_{10}	O	X	X
H_{11}	X	O	X
H_{12}	O	X	X
H_{13}	O	X	X
H_{14}	O	X	X
H_{15}	X	O	X
H_{16}	O	X	X
H_{17}	O	X	X
H_{18}	O	X	X
H_{19}	O	X	X
H_{20}	O	X	X
H_{21}	X	O	X
H_{22}	O	X	X
H_{23}	O	X	X
H_{24}	O	X	X
H_{25}	X	X	O
H_{26}	O	X	X

multitime scale energy dynamics, as summarized in Table 8. The outlet stream of the burner, which has the largest amount of energy among all the process flows, provides energy to other streams through seven heat exchangers and the steam reformer, forming a pseudothroughput in the sense that the throughput starts at a process unit, not an energy source. The energy dynamics of the network is dominated by this large energy throughput, hence the absence of time-scale segregation in the energy dynamics.

Energy-Integrated Distillation Columns

Energy integration in distillation column networks has been an active area of research, as distillation is one of the most energy intensive processes in chemical plants, and has resulted in various thermally coupled configurations.[22] It has been shown that the energy flow structures of such configurations are combinations of energy recycles and energy throughputs, showing a potential for multitime scale dynamics.[15] However, the time scale properties of such configurations are not clear *a priori*. In what follows, we apply the graph-theoretic analysis to two different examples of such networks.

Vapor recompression distillation

Vapor recompression distillation (VRD) represents a typical example of energy-integrated distillation column networks, where the condenser and the reboiler of the same column are thermally coupled. Let us consider the so-called *direct* VRD configuration, where the recompressed vapor stream is directly used to heat the bottom liquid stream, as shown in Figure 11. The top vapor stream of the distillation column is compressed in the compressor to facilitate the heat

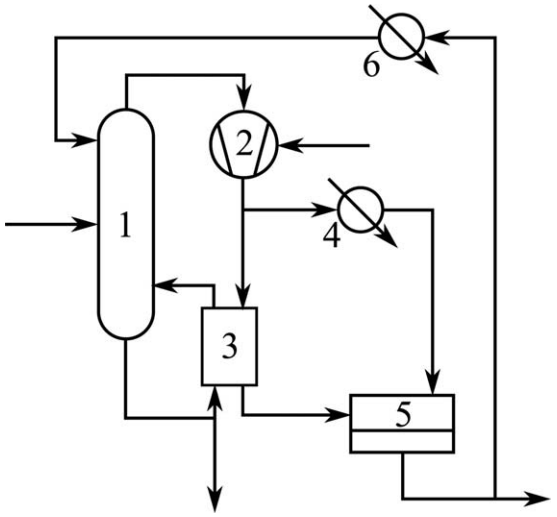

Figure 11. Direct VRD (1: Distillation column, 2: Compressor, 3: Combined reboiler-condenser, 4: Trim condenser, 5: Reflux drum, and 6: Auxiliary cooler).

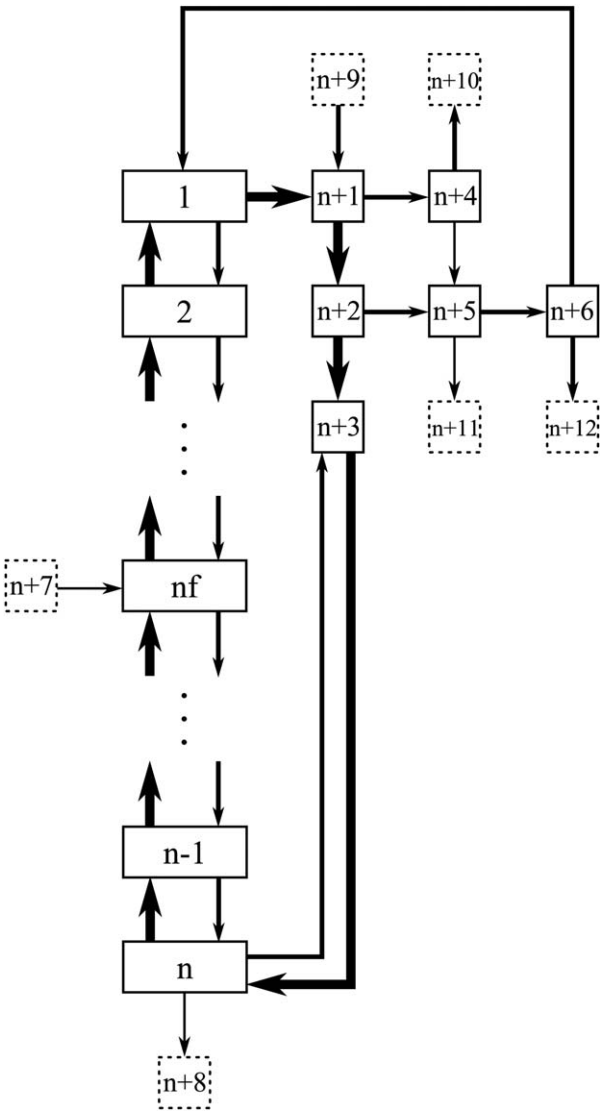

Figure 12. Energy flow graph of direct VRD.

Table 9. Node List of VRD Energy Flow Graph

Normal Nodes		Auxiliary Nodes	
Index	Unit	Index	Unit
1 ∼n	Distillation column	n + 7	Column feed stream
n + 1	Compressor	n + 8	Bottoms stream
n + 2	RC-Condenser	n + 9	Compressor power input
n + 3	RC-Reboiler	n + 10	Trim condenser sink
n + 4	Trim condenser	n + 11	Distillate
n + 5	Reflux drum	n + 12	Auxiliary cooler sink
n + 6	Auxiliary cooler		

Table 10. Summary of Orders of Magnitude of the Energy Flows of the VRD

Energy Flow	Order of Magnitude	Energy Flow	Order of Magnitude
$i + 1 \rightarrow i$, $1 \le i \le 94$	$\mathcal{O}(1/\varepsilon_2)$	$100 \rightarrow 101$	$\mathcal{O}(1/\varepsilon_1)$
$1 \rightarrow 96$	$\mathcal{O}(1/\varepsilon_2)$	$101 \rightarrow 1$	$\mathcal{O}(1/\varepsilon_1)$
$96 \rightarrow 97$	$\mathcal{O}(1/\varepsilon_2)$	$104 \rightarrow 96$	$\mathcal{O}(1/\varepsilon_1)$
$97 \rightarrow 98$	$\mathcal{O}(1/\varepsilon_2)$	$99 \rightarrow 105$	$\mathcal{O}(1/\varepsilon_1)$
$98 \rightarrow 95$	$\mathcal{O}(1/\varepsilon_2)$	$101 \rightarrow 107$	$\mathcal{O}(1/\varepsilon_1)$
$i \rightarrow i + 1$, $1 \le i \le 94$	$\mathcal{O}(1/\varepsilon_1)$	$99 \rightarrow 100$	$\mathcal{O}(1)$
$95 \rightarrow 98$	$\mathcal{O}(1/\varepsilon_1)$	$102 \rightarrow 48$	$\mathcal{O}(1)$
$96 \rightarrow 99$	$\mathcal{O}(1/\varepsilon_1)$	$100 \rightarrow 106$	$\mathcal{O}(1)$
$97 \rightarrow 100$	$\mathcal{O}(1/\varepsilon_1)$	$95 \rightarrow 103$	$\mathcal{O}(1)$

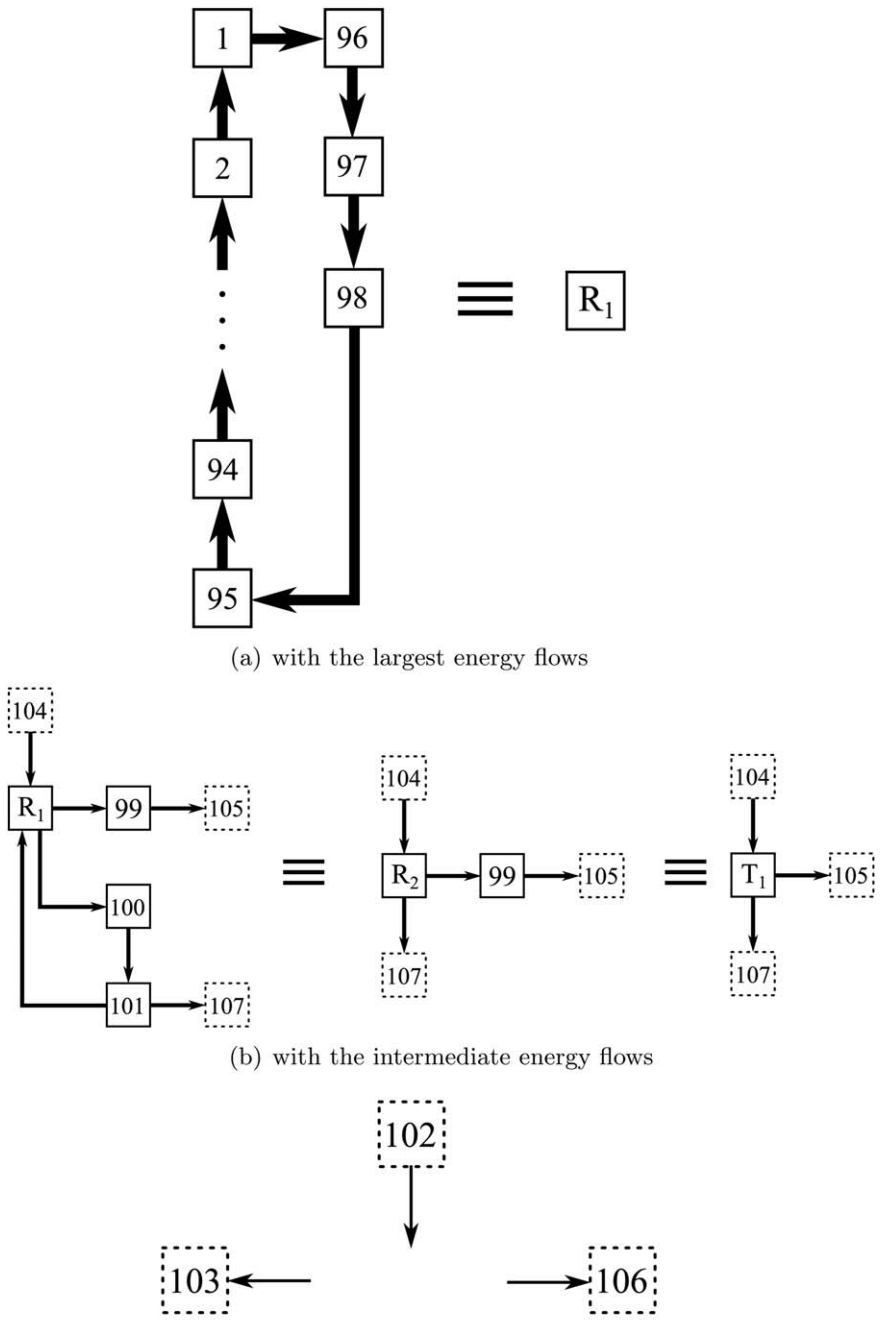

(a) with the largest energy flows

(b) with the intermediate energy flows

(c) with the smallest energy flows

Figure 13. Subgraphs of the VRD energy flow graph.

Table 11. Summary of Time Scale Analysis for the Direct VRD

	Evolution in Each Time Scale		
Enthalpy	Fast	Intermediate	Slow
$H_1 \sim H_{95}$	O	O	X
H_{96}	O	O	X
H_{97}	O	O	X
H_{98}	O	O	X
H_{99}	X	O	X
H_{100}	X	O	X
H_{101}	X	O	X

transfer to the bottoms stream. Then, the majority of the compressed vapor goes through the combined reboiler-condenser to vaporize the bottom liquid stream. The residual vapor is condensed using a trim condenser. An auxiliary cooler is used to regulate the temperature of the reflux. The energy flow structure of this network can be transformed into an energy flow graph $\mathcal{G}$ as shown in Figure 12. Note that the distillation column is represented by n separate nodes each of which corresponds to each tray of the distillation column with *nf* being the feed tray. All the nodes of the energy flow graph are listed in Table 9. The following aspects of this process lead to the segregation in the energy flows:

1. The molar flow rates of the distillate and the bottoms stream are much smaller compared to those of the reflux and the top vapor stream (i.e., there is segregation in the material flows), which results in a difference in the enthalpy content of these streams.

2. The partial molar enthalpy of vapor streams is much larger than the partial molar enthalpy of liquid streams, that is, the latent heat recovered through the combined reboiler-condenser is much larger than the sensible heat of any other energy flow.

In the previous study,[23] a detailed mathematical reduction using singular perturbations was performed, and three-time scale dynamics was documented, with the energy dynamics evolving in the fast and the intermediate time scales and the material dynamics evolving in the intermediate and the slow time scales. For illustration, we consider a column with $n = 95$ and $nf = 47$, and we use the order of magnitude information provided in the Ref. 23, summarized in Table 10.

We apply the proposed graph reduction framework to this network, using the information in Figure 12 and Table 10, focusing on the energy dynamics only. The resulting subgraphs are shown in Figure 13. Figure 13a shows the subgraph $\mathcal{H}_2$ for the energy flows with the largest magnitude $\mathcal{O}(1/\varepsilon_2)$ (corresponding to the fast time scale). The units evolving in the fast time scale are $\mathcal{T}_2 = \{1, 2, \ldots, 97, 98\}$. This subgraph contains one prototype recycle and can be simplified to obtain a single composite recycle node R_1. Figure 13b shows the subgraph $\mathcal{H}_1$ for the energy flow with the intermediate magnitude $\mathcal{O}(1/\varepsilon_1)$ (corresponding to the intermediate time scale). The units evolving in the intermediate time scale are $\mathcal{T}_1 = \{R_1, 99, 100, 101\}$. Note that the composite node R_1 is included in the intermediate time scale, implying that the total enthalpy of the recycle (i.e., $H_1 + H_2 + \cdots + H_{97} + H_{98}$) evolves in the intermediate time scale. A prototype recycle is identified, and can be clustered to form a single composite recycle node R_2. Subsequently, a prototype throughput, which can be replaced by a composite throughput node T_1, is identified, and removed from the energy flow graph before we proceed to the slow time scale. Figure 13c shows the subgraph $\mathcal{H}_0$ for the energy flow with the smallest magnitude $\mathcal{O}(1)$ (corresponding to the slow time scale). Note that this graph contains only the auxiliary nodes and the small energy flows, implying that no enthalpy evolves in this time scale.

Based on the above result, this network is expected to exhibit two-time scale energy dynamics as summarized in Table 11. The canonical forms of the dynamic equations of the original and the reduced models are also obtained. The original model is given as

$$\frac{d\mathbf{H}}{dt} = \mathbf{g}_0 + \frac{1}{\varepsilon_1}\mathbf{g}_1 + \frac{1}{\varepsilon_2}\mathbf{g}_2 \tag{19}$$

with

$$\mathbf{g}_0 = h_{102-48,s}\begin{bmatrix} 0 \\ 0 \\ \vdots \\ 0 \\ k_{102-48}u_{102-48} \\ 0 \\ \vdots \\ 0 \\ -k_{95-103}u_{95-103} \\ 0 \\ 0 \\ 0 \\ -k_{99-100}u_{99-100} \\ k_{99-100}u_{99-100} - k_{100-106}u_{100-106} \\ 0 \end{bmatrix}$$

$$\mathbf{g}_1 = h_{102-48,s}\begin{bmatrix} -k_{1-2}u_{1-2} + k_{101-1}u_{101-1} \\ k_{1-2}u_{1-2} - k_{2-3}u_{2-3} \\ k_{2-3}u_{2-3} - k_{3-4}u_{3-4} \\ \vdots \\ k_{93-94}u_{93-94} - k_{94-95}u_{94-95} \\ k_{94-95}u_{94-95} - k_{95-98}u_{95-98} \\ -k_{96-99}u_{96-99} + k_{104-96}u_{104-96} \\ -k_{97-100}u_{97-100} \\ k_{95-98}u_{95-98} \\ k_{96-99}u_{96-99} - k_{99-105}u_{99-105} \\ k_{97-100}u_{97-100} - k_{100-101}u_{100-101} \\ k_{100-101}u_{100-101} - k_{101-1}u_{101-1} - k_{101-107}u_{101-107} \end{bmatrix}$$

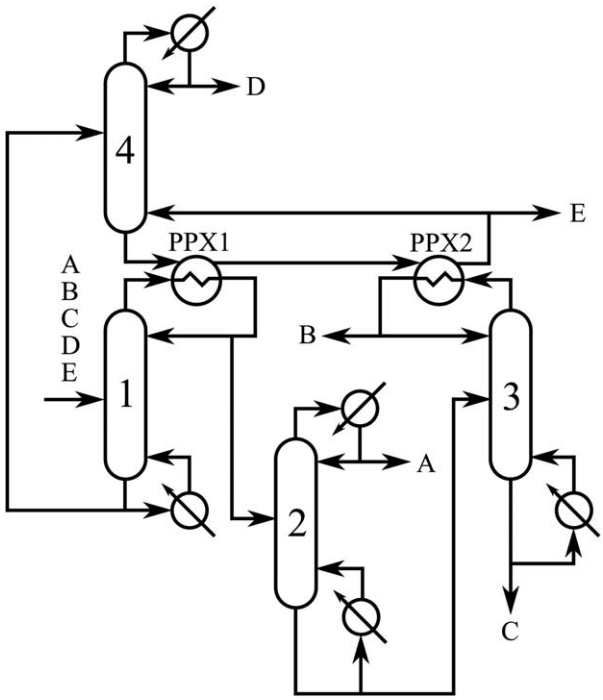

Figure 14. Heat-integrated distillation column network for five-component separation.

$$\mathbf{g}_2 = h_{102-48,s}\begin{bmatrix} -k1-96u_{1-96}+k_{2-1}u_{2-1} \\ -k_{2-1}u_{2-1}+k_{3-2}u_{3-2} \\ -k_{3-2}u_{3-2}+k_{4-3}u_{4-3} \\ \vdots \\ -k_{94-93}u_{94-93}+k_{95-94}u_{95-94} \\ -k_{95-94}u_{95-94}+k_{98-95}u_{98-95} \\ -k_{1-2}u_{1-2}+k_{4-1}u_{4-1} \\ k_{1-96}u_{1-96}-k_{96-97}u_{96-97} \\ k_{96-97}u_{96-97}-k_{97-98}u_{97-98} \\ k_{97-98}u_{97-98}-k_{98-95}u_{98-95} \\ 0 \\ 0 \\ 0 \end{bmatrix}$$

k_{i-j} in $\mathbf{g}_0$, $\mathbf{g}_1$ and $\mathbf{g}_2$, which are the $\mathcal{O}(1)$ steady state ratios, are defined as

$$k_{i-j}=\frac{h_{i-j,s}}{h_{8-1,s}},\quad \frac{h_{i-j,s}}{h_{95-98,s}},\quad \frac{h_{i-j,s}}{h_{1-96,s}}$$

repectively, whereas u_{i-j} are defined as

$$u_{i-j}=\frac{h_{i-j}}{h_{i-j,s}}$$

where h_{i-j} represents the energy flow from the i-th unit to the j-th unit, and the subscript s denotes a steady state value. ε_1 and ε_2 are small parameters, which are the ratios of the nominal energy input through the feed stream (i.e., $h_{8-1,s}$) to the nominal energy flow from the distillation column to the reboiler (i.e., $h_{95-98,s}$) and to the compressor (i.e., $h_{1-96,s}$), respectively.

The fast time scale dynamics is given as

$$\frac{d\mathbf{H}_2}{d\tau_2}=\mathbf{F}_2^T\mathbf{g}_2=\mathbf{g}_2'$$

with

$$\mathbf{F}_2=\begin{bmatrix}\mathbf{I}_{98\times 98}\\ \mathbf{0}_{3\times 98}\end{bmatrix}$$

where $\mathbf{H}_2=\{H_1,H_2,\ldots,H_{97},H_{98}\}$ and $\tau_2=t/\varepsilon_2$ is a stretched fast time scale. The quasi-steady state constraints, $\mathbf{g}_2'=0$, are identified as linearly dependent.

The intermediate time scale dynamics is given in DAE form as

$$\frac{d\mathbf{H}_1}{d\tau_1}=\mathbf{g}_1+\mathbf{F}_2\mathbf{B}_2\bar{\mathbf{z}}_2$$

$$\tilde{\mathbf{g}}_2'=0$$

with

$$\mathbf{B}_2=\begin{bmatrix}\mathbf{I}_{97\times 97}\\ -\mathbf{1}_{1\times 97}\end{bmatrix}$$

where $\mathbf{H}_1=\{H_1,H_2,\ldots,H_{100},H_{101}\}$. $\tilde{\mathbf{g}}_2'$ represents the subset of linearly independent constraints given as $\mathbf{g}_2'=\mathbf{B}_2\tilde{\mathbf{g}}_2'$. $\bar{\mathbf{z}}_2$ is a vector of algebraic variables, defined by

$$\lim_{\varepsilon_2\to 0}\frac{\tilde{\mathbf{g}}_2'}{\varepsilon_2}$$

The quasi-steady state constraints for the intermediate time scale are identified as $\mathbf{g}_1+\mathbf{F}_2\mathbf{B}_2\bar{\mathbf{z}}_2=0$, which are linearly independent. This is consistent with the fact that the energy dynamics of the network does not evolve in the slow time scale.

Note that the above equations have exactly the same canonical forms with the equations derived using the detailed mathematical analysis within the framework of singular perturbations in the Ref. 23.

Remark 2. *The distillation column can be represented as a single node (instead of separate nodes for each tray) to analyze the time scale property of the dynamics of the overall enthalpy of the column. In this case, we obtain one*

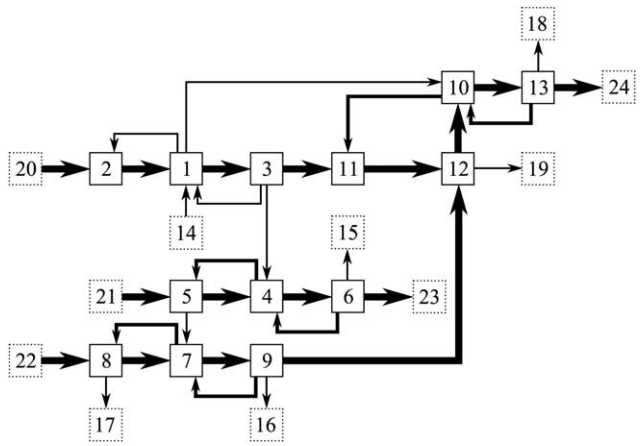

Figure 15. Energy flow graph of five-component separation.

Table 12. Node List of Five-Component Separation Energy Flow Graph

Normal Nodes		Auxiliary Nodes	
Index	Unit	Index	Unit
1	Distillation column 1	14	Feed stream
2	DC1-Reboiler	15	Product stream (A)
3	PPX1-Hot	16	Product stream (B)
4	Distillation column 2	17	Product stream (C)
5	DC2-Reboiler	18	Product stream (D)
6	DC2-Condenser	19	Product stream (E)
7	Distillation column 3	20	DC1-Reboiler source
8	DC3-Reboiler	21	DC2-Reboiler source
9	PPX2-Hot	22	DC3-Reboiler source
10	Distillation column 4	23	DC2-Condenser sink
11	PPX1-Cold	24	DC4-Condenser sink
12	PPX2-Cold		
13	DC4-Condenser		

Table 13. Summary of Orders of Magnitude of the Energy Flows of Five-Component Separation Network

Energy Flow	Order of Magnitude	Energy Flow	Order of Magnitude
$2 \rightarrow 1$	$\mathcal{O}(1/\varepsilon_2)$	$7 \rightarrow 8$	$\mathcal{O}(1/\varepsilon_1)$
$1 \rightarrow 3$	$\mathcal{O}(1/\varepsilon_2)$	$9 \rightarrow 7$	$\mathcal{O}(1/\varepsilon_1)$
$5 \rightarrow 4$	$\mathcal{O}(1/\varepsilon_2)$	$10 \rightarrow 11$	$\mathcal{O}(1/\varepsilon_1)$
$4 \rightarrow 6$	$\mathcal{O}(1/\varepsilon_2)$	$13 \rightarrow 10$	$\mathcal{O}(1/\varepsilon_1)$
$8 \rightarrow 7$	$\mathcal{O}(1/\varepsilon_2)$	$14 \rightarrow 1$	$\mathcal{O}(1)$
$7 \rightarrow 9$	$\mathcal{O}(1/\varepsilon_2)$	$1 \rightarrow 2$	$\mathcal{O}(1)$
$3 \rightarrow 11$	$\mathcal{O}(1/\varepsilon_2)$	$3 \rightarrow 1$	$\mathcal{O}(1)$
$9 \rightarrow 12$	$\mathcal{O}(1/\varepsilon_2)$	$1 \rightarrow 10$	$\mathcal{O}(1)$
$11 \rightarrow 12$	$\mathcal{O}(1/\varepsilon_2)$	$6 \rightarrow 15$	$\mathcal{O}(1)$
$12 \rightarrow 10$	$\mathcal{O}(1/\varepsilon_2)$	$9 \rightarrow 16$	$\mathcal{O}(1)$
$10 \rightarrow 13$	$\mathcal{O}(1/\varepsilon_2)$	$8 \rightarrow 17$	$\mathcal{O}(1)$
$4 \rightarrow 5$	$\mathcal{O}(1/\varepsilon_1)$	$13 \rightarrow 18$	$\mathcal{O}(1)$
$6 \rightarrow 4$	$\mathcal{O}(1/\varepsilon_1)$	$12 \rightarrow 19$	$\mathcal{O}(1)$

equation for the dynamics of the distillation column, along with six equations for the other process units, instead of a set of equations which describe the energy dynamics of each tray of the distillation column.

Also, the controlled outputs and the potential manipulated inputs available for each time scale can be readily identified. The enthalpies of the distillation column, the compressor, and the combined reboiler-condenser need to be controlled in the fast time scale (τ_2), and all but one out of four units should be controlled (i.e., $\mathcal{Y}(\tau_2)=\{1,2,\ldots,97,98\}$) as no auxiliary node is connected to R_1 in $\mathcal{H}_2$. Potential manipulated inputs in this time scale include: $\mathcal{U}(\tau_2)=\{1-96, 2-1, 3-2, \ldots, 95-94, 96-97, 97-98, 98-95\}$.

The enthalpies of the trim condenser, the reflux drum, and the auxiliary cooler as well as the total enthalpy of R_1 need to be controlled in the intermediate time scale (i.e., $\mathcal{Y}(\tau_1)=\{R_1, 99, 100, 101\}$). The following set of potential manipulated inputs is identified: $\mathcal{U}(\tau_1)=\{96-99, 97-100, 99-105, 100-101, 101-1, 101-107, 104-96\}$.

The reduced models obtained above can be used for deriving nonlinear model-based controllers for each time scale, resulting in a hierarchical control strategy. Such controllers are well suited for achieving robust transition performance of the overall system (see the Ref. 23 for example case studies).

Heat-integrated network of distillation columns

Let us consider a distillation column network shown in Figure 14, which was proposed as a solution to a five-component separation problem.[24] In this configuration, four distillation columns are used, and the condensers of the first and third columns are combined with the reboiler of the fourth column through two process-to-process heat exchangers (PPX1 and PPX2). The energy flow graph of the network is shown in Figure 15. The node list is provided in Table 12. The orders of magnitude of the energy flows are determined following the information provided in the Ref. 15, and are summarized in Table 13. We note that the energy flows of the network span three different orders of magnitude. ε_1 and ε_2 are small parameters ($\varepsilon_2 \ll \varepsilon_1 \ll 1$), which are the ratios of the nominal values of the energy input through the feed stream to the energy of the reflux of the distillation column 2, and the duty of the reboiler of the distillation column 1, respectively

$$\varepsilon_1 = \frac{h_{14-1,s}}{h_{6-4,s}}$$

$$\varepsilon_2 = \frac{h_{14-1,s}}{h_{20-2,s}}$$

We feed the information in Figure 15 and Table 13 to the graph reduction algorithm. Figure 16 shows the obtained subgraphs of the network corresponding to each time scale. In the fast time scale subgraph, three large throughputs (from the node 21 to the node 23, from the node 22 to the node 24 and from the node 20 to the node 24) are identified, and these throughputs need to be removed from the energy flow graph before we proceed to the slower time scales as

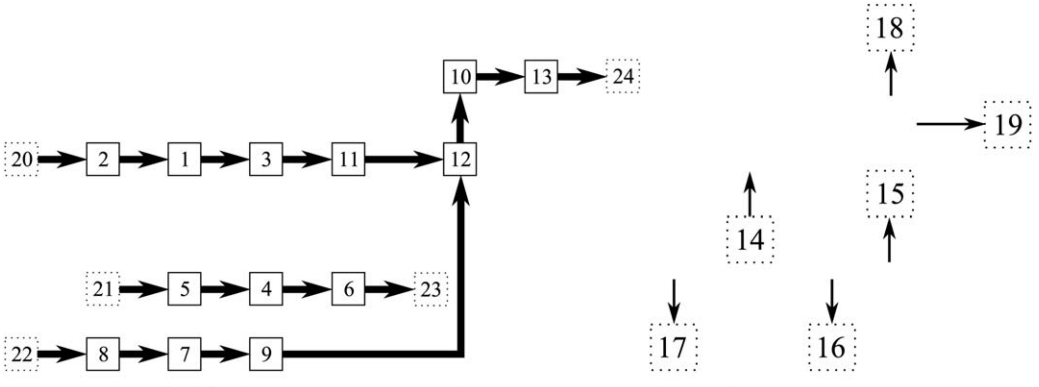

Figure 16. Subgraphs of the five-component separation energy flow graph.

all the units in the throughput evolve in a single time scale (fast time scale in this case). Note that all the normal nodes are parts of at least one of three throughputs. The intermediate time scale subgraph is empty, and thus, not shown here. Also note that, in the slow time scale subgraph, we only have the energy flows of the smallest magnitude, and the auxiliary nodes, implying that no unit evolves in those time scales.

In summary, the energy dynamics of this network is mainly driven by the large energy throughputs, with the energy dynamics of every process unit evolving in the fast time scale. This implies that no time scale hierarchy in the energy dynamics exists that could be used to address energy management. This is a common feature in such networks due to the existence of large energy sources/sinks forming large energy throughputs.

In the cases where we do not have multitime scale energy dynamics, we cannot implement a hierarchical control strategy as we did for the VRD and HDA examples. For such cases, one can seek a way to *decompose* the network into smaller subnetworks such that the units in the same subnetwork interact strongly with each other, whereas the units in different subnetworks interact weakly. Then, separate controllers for each subnetwork can be designed, resulting in a quasi-decentralized control structure.

Conclusions and Discussion

In this article, we illustrated the main features of a graph reduction method that we have developed to analyze complex energy-integrated chemical processes. Specifically, using the connectivity information and the order of magnitude information as the inputs, the method can be used to identify the time scales exhibited by the networks, to obtain the canonical forms of the original and the reduced dynamic models, and to classify the controlled outputs and the potential manipulated inputs available in each time scale.

We applied the framework to two different classes of complex energy-integrated networks: distillation column networks and reactor-heat exchanger networks. For each class, we analyzed two example networks, one of which turned out to exhibit multitime scale dynamics, whereas the other did not. For the HDA example, we performed a detailed mathematical analysis using singular perturbations as the model reduction tool, as well as open-loop numerical simulations, to validate the results obtained using the framework. For the VRD example, we compared the results obtained using the framework with the results documented in the existing literature, which was obtained using a detailed mathematical analysis within the framework of singular perturbations.

The proposed method has several advantages over a detailed mathematical analysis. First, it is scalable and easily applicable to large complex networks. Also, the graph theory algorithms are efficient and automated (it takes less than a second, for all the cases, to run the algorithm on a quad core Intel Xeon 3.2GHz 64-bit processor). Moreover, information only on the connectivity of the network and the orders of magnitude of the energy flows is required. The method can be used to develop hierarchical control structures in cases with a segregation of energy flows leading to multiple time scales, or to document that such multiplicity does not exist.

The graph-theoretic framework that we have developed is currently being extended to complex networks combining energy and material integration.

Acknowledgments

Financial support for this work by the National Science Foundation, grant CBET-1133167, is gratefully acknowledged.

Literature Cited

1. Yee TF, Grossmann IE, Kravanja Z. Simultaneous optimization models for heat integration—I. Area and energy targeting and modeling of multi-stream exchangers. *Comput Chem Eng*. 1990;14(10):1151–1164.
2. Westerberg AW. A retrospective on design and process synthesis. *Comput Chem Eng*. 2004;28(4):447–458.
3. Ydstie BE. Passivity based control via the second law. *Comput Chem Eng*. 2002;26(7):1037–1048.
4. Hudon N, Bao J. Dissipativity-based decentralized control of interconnected nonlinear chemical processes. *Comput Chem Eng*. 2012;45:84–101.
5. Tippett MJ, Bao J. Distributed model predictive control based on dissipativity. *AIChE J*. 2013;59(3):787–804.
6. Rawlings JB, Stewart BT. Coordinating multiple optimization-based controllers: new opportunities and challenges. *J Process Control*. 2008;18(9):839–845.
7. Liu J, Muñoz de la Peña D, Christofides PD. Distributed model predictive control of nonlinear process systems. *AIChE J*. 2009;55(5):1171–1184.
8. Mhaskar P, Gani A, McFall C, Christofides PD, Davis JF. Fault-tolerant control of nonlinear process systems subject to sensor faults. *AIChE J*. 2007;53(3):654–668.
9. Sun Y, El-Farra NH. Quasi-decentralized model-based networked control of process systems. *Comput Chem Eng*. 2008;32(9):2016–2029.
10. Luyben ML, Tyreus BD, Luyben WL. Plantwide control design procedure. *AIChE J*. 1997;43(12):3161–3174.
11. Skogestad S. Control structure design for complete chemical plants. *Comput Chem Eng*. 2004;28(1):219–234.
12. Jogwar SS, Baldea M, Daoutidis P. Dynamics and control of process networks with large energy recycle. *Ind Eng Chem Res*. 2009;48(13):6087–6097.
13. Scattolini R. Architectures for distributed and hierarchical model predictive control: a review. *J Process Control*. 2009;19(5):723–731.
14. Baldea M, Daoutidis P. Modeling, dynamics and control of process networks with high energy throughput. *Comput Chem Eng*. 2008;32(9):1964–1983.
15. Jogwar SS, Daoutidis P. Energy flow patterns and control implications for integrated distillation networks. *Ind Eng Chem Res*. 2010;49(17):8048–8061.
16. Jogwar SS, Rangarajan S, Daoutidis P. Multi-time scale dynamics in energy-integrated networks: a graph theoretic analysis. In: *IFAC World Congress*, Milano, Italy, Vol. 18, 2011:6085–6090.
17. Heo S, Jogwar SS, Rangarajan S, Daoutidis P. Graph reduction for hierarchical control of energy integrated process networks. In: *2012 IEEE 51st Annual Conference on Decision and Control (CDC)*, Maui, HI, 2012:6388–6393.
18. Terrill D, Douglas J. Heat-exchanger network analysis. 1. Optimization. *Ind Eng Chem Res*. 1987;26(4):685–691.
19. Heo S, Georgis D, Daoutidis P. Control structure design for complex energy integrated networks using graph-theoretic methods. In: *2013 IEEE 21st Mediterranean Conference on Control & Automation (MED)*, Platanias-Chania, Greece, 2013:477–482.
20. Zimmerman CC, York R. Thermal demethylation of toluene. *Ind Eng Chem Process Des Dev*. 1964;3(3):254–258.
21. Georgis D, Jogwar SS, Almansoori AS, Daoutidis P. Design and control of energy integrated SOFC systems for *in situ* hydrogen production and power generation. *Comput Chem Eng*. 2011;35(9):1691–1704.
22. Annakou O, Mizsey P. Rigorous comparative study of energy-integrated distillation schemes. *Ind Eng Chem Res*. 1996;35(6):1877–1885.
23. Jogwar SS, Daoutidis P. Dynamics and control of vapor recompression distillation. *J Process Control*. 2009;19(10):1737–1750.
24. Andrecovich M, Westerberg A. An MILP formulation for heat-integrated distillation sequence synthesis. *AIChE J*. 1985;31(9):1461–1474.

Appendix: A Graph-Theoretic Algorithm for the Analysis of Complex Energy-Integrated Networks

Algorithm: *ComplexNetworkAnalysis*$(\mathcal{G}, W)$

1. Sort W in descending order
2. **for** i=1 to Size(W)=m **do**
3. μ = W[i]
4. $\mathbf{g}_\mu(\mathbf{u}_\mu)=h_{1,s} \times Ebalance(\mathcal{G}, \mu)$;
5. $\mathcal{H}_\mu = InducedSubgraph(\mathcal{G}, \mu)$
6. $\mathcal{T}(\tau_\mu)$ = nodes $\in \mathcal{H}_\mu$
7. **for** each node N $\in \mathcal{H}_\mu$ **do**
8. **if** N is a composite node then
9. add $\sum N[k]$ to $\mathcal{Y}(\tau_\mu)$
10. **else**
11. add N to $\mathcal{Y}(\tau_\mu)$
12. **end if**
13. **end for**
14. $\mathcal{U}(\tau_\mu)$ = Edges in $\mathcal{H}_\mu$
15. C = *SmallestElementaryCycle*$(\mathcal{H}_\mu)$
16. **while** C $\neq \phi$ **do**
17. *GraphReduce*$(\mathcal{G}$,C,$\mu)$
18. *GraphReduce* $(\mathcal{H}_\mu$,C,$\mu)$
19. C = *SmallestElementaryCycle*$(\mathcal{H}_\mu)$
20. **end while**
21. **if** size(RecycleTimes) $\neq 0$ **then**
22. $DAE_\mu=\mathbf{C}_{\mu^-}\mathbf{B}_{\mu^-}\mathbf{z}_{\mu^-}$
23. $Constraint_\mu=\tilde{\mathbf{g}}_{\mu^-}(\mathbf{u}_{\mu^-})$
24. **if** size(RecycleTimes) >1 **then**
25. $AddConstraints_\mu=\sum_{j=1}^{size(RecycleTimes)} DAE_j$
26. **end if**
27. **end if**
28. **if** degree(N) =0 for any node N $\in \mathcal{H}_\mu$ **then**
29. Add τ_μ to RecycleTimes
30. Add N_j to PureRecycles
31. All but 1 out of N_j should be controlled in this time scale
32. **end if**
33. **if** degree(N) $\neq$ 0 for all nodes N $\in \mathcal{H}_\mu$ **then**
34. Clear RecycleTimes, PureRecycles
35. **end if**
36. **for all** node N $\in \mathcal{H}_\mu$ such that degree(N) $\neq$ 0 **do**
37. **if** N is a composite node then
38. Remove $N[k]$ from PureRecycles
39. **end if**
40. Remove N from $\mathcal{G}$
41. **end for**
42. **end for**
43. Energy balance equations are
44. $$\frac{d\mathbf{H}}{dt}=\sum_{\mu=W[1]}^{W[m]}\frac{1}{\varepsilon_\mu}\mathbf{g}_\mu(\mathbf{H},\mathbf{u}_\mu)$$
45. **for all** $\mu \in W$ **do**
46. Reduced order model in τ_μ is
47. $$\frac{d\mathbf{H}_\mu}{d\tau_\mu}=\overline{\mathbf{g}}_\mu(\mathbf{H},\mathbf{u}_\mu)+DAE_\mu$$
$$0=Constraint_\mu+AddConstraints_\mu$$
48. **end for**
49. **return** $\mathcal{T},\mathcal{Y},\mathcal{U}$

Manuscript received Aug. 21, 2013, and revision received Dec. 16, 2013.